Mon. Not. R. Astron. Soc. **378,** 801–818 (2007) doi:10.1111/j.1365-2966.2007.11847.x

Coincident, 100 kpc scale damped Lyα absorption towards a binary QSO: how large are galaxies at $z \sim 3$?

Sara L. Ellison,[1⋆] Joseph F. Hennawi,[2†] Crystal L. Martin[3‡] and Jesper Sommer-Larsen[4,5]

[1]Department Physics & Astronomy, University of Victoria, 3800 Finnerty Road, Victoria, BC, Canada V8P 1A1
[2]Department Physics & Astronomy, University of California, Berkeley, USA
[3]Department Physics & Astronomy, University of California, Santa Barbara, USA
[4]Dark Cosmology Centre, Niels Bohr Institute, Juliane Maries Vej 30, DK-2100 Copenhagen Ø, Denmark
[5]Institute of Astronomy, University of Tokyo, Osawa 2-21-1, Mitaka, Tokyo 181-0015, Japan

Accepted 2007 April 12. Received 2007 April 11; in original form 2006 December 14

ABSTRACT

We report coincident damped Lyα (DLA) and sub-DLA absorption at $z_{\rm abs} = 2.66$ and $z_{\rm abs} = 2.94$ towards the $z \sim 3$, 13.8 arcsec separation binary quasar SDSS 1116+4118 AB. At the redshifts of the absorbers, this angular separation corresponds to a proper transverse separation of $\sim$110 h_{70}^{-1} kpc. A third absorber, a sub-DLA at $z_{\rm abs} = 2.47$, is detected towards SDSS 1116+4118 B, but no corresponding high column density absorber is present towards SDSS 1116+4118 A. We use high-resolution galaxy simulations and a clustering analysis to interpret the coincident absorption and its implications for galaxy structure at $z \sim 3$. We conclude that the common absorption in the two lines of sight is unlikely to arise from a single galaxy, or a galaxy plus satellite system, and is more feasibly explained by a group of two or more galaxies with separations $\sim$100 kpc. The impact of these findings on single line-of-sight observations is also discussed; we show that abundances of DLAs may be affected by up to a few tenths of a dex by line-of-sight DLA blending. From a Keck Echellette Spectrograph and Imager spectrum of the two quasars, we measure metal column densities for all five absorbers and determine abundances for the three absorbers with log N(H I) > 20. For the two highest N(H I) absorbers, we determine high levels of metal enrichment, corresponding to 1/3 and 1/5 $Z_\odot$. These metallicities are amongst the highest measured for DLAs at any redshift and are consistent with values measured in Lyman-break galaxies at $2 < z < 3$. For the DLA at $z_{\rm abs} = 2.94$ we also infer an approximately solar ratio of α-to-Fe peak elements from [S/Zn] = +0.05, and measure an upper limit for the molecular fraction in this particular line of sight of $\log f(\mathrm{H}_2) < -5.5$.

Key words: galaxies: abundances – galaxies: high-redshift – quasars: absorption lines.

1 INTRODUCTION

For the last decade, a simple schematic view of the relative sizes of QSO absorption systems has been built on the coupling of absorbers with galaxies of varying luminosities and impact parameters and the consideration of luminosity functions and number densities (e.g. Lanzetta 1993; Steidel 1993, 1995). Although a galaxy's gas cross-section depends on its individual properties (such as mass and luminosity), the topology of a given galaxy is usually considered to be hierarchical and based on column density (e.g. Steidel 1993; Churchill, Kacprzak & Steidel 2005). In this picture, the damped Lyα (DLA) systems represent a relatively small fraction of a galaxy's gas cross-section, associated with its inner $\sim$10–20 kpc. The Mg II bearing gas, associated with Lyman-limit systems, occupies a somewhat larger halo; in the original Steidel (1995) picture this halo was roughly spherical, had a covering factor of approximately unity and a radius $\sim$40 kpc for an $L^\star$ galaxy. The largest absorption cross-section was associated with C IV absorbing gas and extended out to distances of the order of 100 kpc. Although attractive in its simplicity, this picture has recently undergone significant re-evaluation. For example, although the idea of large C IV haloes has been vindicated by observations of absorbers near to Lyman-break galaxies (LBGs; Adelberger et al. 2003, 2005b), it has been

⋆E-mail: sarae@uvic.ca
†Hubble Fellow.
‡Packard Fellow.

argued that some C IV absorbers may be associated with a more diffuse component, possibly the intergalactic medium (Pieri, Schaye & Aguirre 2006). Structure has also been inferred in the Mg II population. Ellison et al. (2004b) argued that variations in Mg II equivalent widths (EWs) on kpc scales seen in spatially resolved lensed QSO images suggest individual Mg II 'clouds' that are an order of magnitude smaller than the halo sizes found by previous galaxy surveys. Even the sizes of the Mg II haloes are currently being re-assessed; it has been suggested by Churchill, Kacprzak & Steidel (2005) that the original survey strategies may have led to an underestimate of the extent of the absorbing gas.

In light of these recent re-evaluations, it may be surprising how little progress we have made in determining the sizes of DLAs. These are probably the best studied of the quasar absorption-line menagerie, partially because of the numerous chemical elements that can be used to infer their star formation histories (e.g. Dessauges-Zavadsky et al. 2004). Unlike the case for C IV and Mg II absorbers, there is scant data from which we can directly infer DLA sizes. The two main techniques that have previously been used for this estimation, namely, the association of individual galaxies with absorbers and the application of lensed QSOs are not yet on a solid statistical footing. The former of these techniques requires a relatively large sample of DLAs with known galaxy counterparts. Although Chen & Lanzetta (2003) attempted this with a sample of six galaxies, the statistics are poor and only available for $z < 1$, whereas the vast majority of known DLAs are at $z > 2$ (e.g. Prochaska, Herbert-Fort & Wolfe 2005). At higher redshifts, only Møller, Fynbo & Fall (2004) and Weatherley et al. (2005) have made direct detections of DLAs and find impact parameters in the range 2–25 h_{70}^{-1} kpc for three DLAs. Measurements of DLA sizes from lensed QSOs are currently limited by the very small number (4) of DLAs that have been detected in lensed sightlines and by the small transverse scales that they probe. Two out of the four cases (Kobayashi et al. 2002; Churchill et al. 2003) probe very small scales (<250 pc), leaving only two measurements on kpc scales ($d \sim 5$ kpc by Lopez et al. 2005 and $d \sim 10$ kpc by Smette et al. 1995). A few indirect limits of DLA sizes also exist, for example, lower limits based on extended background radio emission (e.g. Foltz et al. 1988; Briggs et al. 1989) or on the unique case of transverse Lyα fluorescence discovered by Adelberger et al. (2006). It is also possible to estimate gas cross-sections by combining the DLA number density with a Holmberg relation between the radius of a disc and the galaxy luminosity (e.g. Fynbo, Møller & Warren 1999). The disadvantage of this approach is that it assumes a specific and fixed geometry, although like other methods, it gives typical disc sizes up to ~30 kpc. Apart from this handful of direct and indirect constraints, the scenario in which DLAs have cross-sections of a few tens of kpc has been largely untested.

In this paper, we present observations of a close binary QSO, SDSS 1116+4118 AB, hereafter QSO A/B, with an angular separation between the two components (both at $z \sim 3$) of 13.8 arcsec, see Table 1 and Fig. 1. QSO B exhibits three high column density, intervening absorbers, two of which are also detected in QSO A, even though the proper separation at the redshift of the absorbers is more than 100 h_{70}^{-1} kpc. In order to interpret this result, we use high-resolution smoothed particle hydrodynamic (SPH) simulations of two galaxies at $z = 2.3, 3.0, 3.6$ to assess whether a structure as large as 100 h_{70}^{-1} kpc is likely to be a single galaxy, a satellite system or a group of galaxies and discuss the implications of these possibilities.

Table 1. Target properties.

QSO	RA (J2000)	Dec. (J2000)	i (mag)	$z_{\rm em}$
SDSS 1116+4118 A	11 16 11.7	41 18 21.5	17.97	2.982 ± 0.007
SDSS 1116+4118 B	11 16 10.7	41 18 14.4	19.00	3.007 ± 0.007

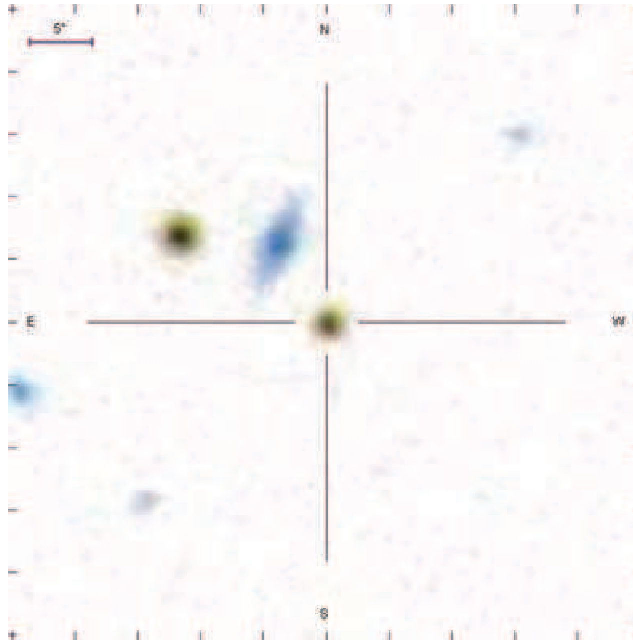

Figure 1. SDSS image of the binary QSO SDSS1116+4118 AB. QSO B is at the centre of the image and QSO A is offset by 13.8 arcsec to the north-east. The galaxy located between the two QSO images does not have a spectroscopic redshift, but Sanchez-Alvaro & Rodriguez-Calonge (2007) give a photometric redshift of $z = 0.25$.

We adopt a cosmology of $\Omega_\Lambda = 0.7, \Omega_{\rm M} = 0.3$ and $H_0 = 70$ km s^{-1} Mpc^{-1}. In this cosmology, redshifts of 2.47, 2.66 and 2.94 (the redshifts of the absorbers studied in this paper) 1 arcsec in the transverse direction corresponds to proper linear distances of 8.09, 7.96 and 7.75 h_{70}^{-1} kpc, respectively.

2 OBSERVATIONS AND DATA ANALYSIS

Although the Sloan Digital Sky Survey (SDSS) spectroscopic quasar survey has provided the largest sample (~10^5) of quasars in existence, it selects *against* close quasar pairs due to the finite size of optical fibres in the multi-object spectrograph. This fibre collision limit implies that only one member of a pair with $\Delta\theta < 1$ arcmin will make it into the quasar catalogue. Hennawi et al. (2006a) selected a large sample of candidate close companions around the SDSS quasars using photometric redshift techniques, and spectroscopically confirmed them to be quasar pairs with follow-up observations at low spectral resolution. A small number of QSO pairs can also be discovered when there is plate overlap for a given field. In this case, fibres can be placed on very closely spaced objects in two different plates. The QSO pair SDSS 1116+4118 AB falls into this latter category; an SDSS postage stamp of the field is shown in Fig. 1 and shows both QSOs as well as a foreground galaxy. For a sample of spectroscopically confirmed QSO pairs, we are currently undertaking higher resolution spectra in order to study the transverse absorption properties of intervening galaxies and the intergalactic medium. The data presented here were obtained as part of that systematic study and they represent the only pair for which we have currently detected a DLA in either line of sight (many of the spectra do not have large Lyα forest coverage).

Sanchez-Alvaro & Rodriguez-Calonge (2007) have recently proposed SDSS 1116+4118 AB to be a wide separation lens, with the foreground galaxy (whose photometric redshift is given as $z = 0.25$) as the lensing mass. However, we consider this unlikely due to (i) the improved redshift determinations of the two QSOs (Table 1) which are significantly different: the C IV emission lines are offset by 36 Å; (ii) the considerable differences between QSO A and B in our Echellette Spectrograph and Imager (ESI) spectra, both in absorption and emission characteristics; (iii) the extremely low likelihood that a single galaxy would produce such a wide separation image (the implied mass-to-light ratio is >100 at the Einstein radius); (iv) lack of counter images on north side of the lens galaxy (the offset lens should produce a quadruple image); (v) high-redshift ($z > 2.5$) C IV absorbers show large fractional EW differences ($\gg$50 per cent) between QSO A and B, inconsistent with lensing-predicted line-of-sight separations of $\leqslant 1.5\,h_{70}^{-1}$ kpc (e.g. Lopez, Hagen & Reimers 2000; Rauch, Sargent & Barlow 2001a; Rauch et al. 2001b; Ellison et al. 2004b) and (vi) the inconsistency of QSO colours, for example, $g - i = 0.61 \pm 0.02$ and 0.45 ± 0.02 for A and B, respectively. Only the presence of a massive cluster would cause such wide separation multiple images, such as the recently discovered 14 arcsec separation quadruply imaged SDSS 1004+4112 (Inada et al. 2003) where the estimated cluster mass is $M \sim 10^{14}\,\mathrm{M}_{\odot}$ (Oguri et al. 2004). No such cluster is seen in the SDSS images of SDSS 1116+4118, or in deeper Multi-Mirror Telescope (MMT) images (A. Marble, private communication). We therefore assume that SDSS 1116+4118 AB is a projected pair of QSOs.

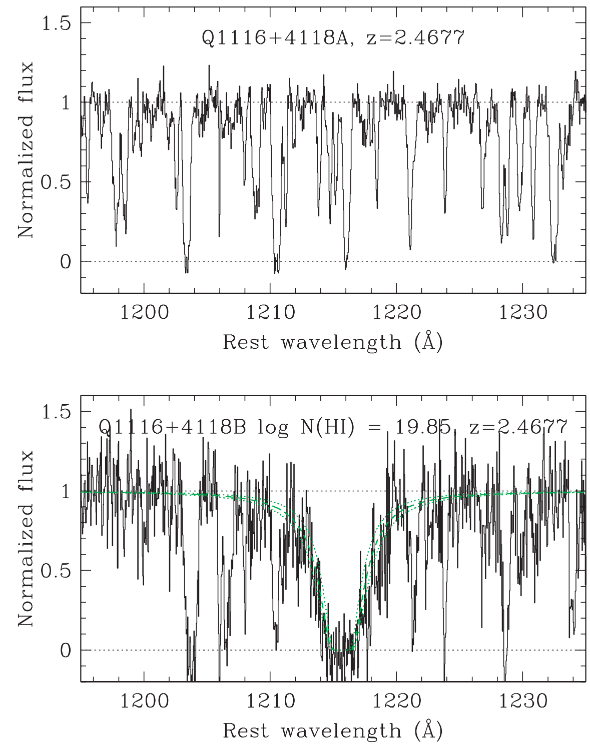

Figure 2. Lyα fit (dashed profile) and error (dotted profiles) to the $z_{\rm abs} \sim 2.47$ sub-DLA seen towards QSO B (bottom panel), but not towards QSO A (top panel). The transverse separation of the two sightlines at this redshift is 112 h_{70}^{-1} kpc.

2.1 Data acquisition and reduction

On 2006 March 3 we obtained 3300 s of integration in two exposures on QSO A/B using the ESI (Sheinis et al. 2002) on the Keck telescope. Since the entrance slit of the spectrograph is 20 arcsec long, the position angle was chosen so that both QSOs A and B were covered (see Fig. 1). The observing conditions were relatively poor, with high humidity and seeing typically 1.3 arcsec. The data quality was further degraded by broad absorption patterns across many echelle orders due to condensation on the Dewar window caused by observing in high humidity. None the less, with a 1 arcsec slit width and 1 × 1 binning the signal-to-noise ratios (S/N) per pixel were ∼50 in QSO A and 30 in QSO B at 6000 Å.

The data were reduced using a customized version of ESIREDUX[1] which was adapted to deal with multiple objects on the slit. Extracted spectra were calibrated to a vacuum heliocentric wavelength scale and determined to have full width at half-maximum (FWHM) resolutions of $\sim$60 km s^{-1} ($R \sim 5000$). The spectra from the two individual exposures were combined by weighting according to S/N. The QSO continuum (including the broad absorption features induced by the residue on the Dewar window) was estimated with the Starlink software DIPSO[2] by fitting a cubic spline polynomial through unabsorbed regions of flux. To test the effect of the residue, we measure the EWs of unsaturated absorption lines that fall in this region of the spectrum. In theory, dividing the spectrum by the continuum function should not alter the EWs, if the fitting is accurate. We find EWs that agree to within less than a few per cent, indicating that the broad absorption does not affect our line measurements.

We identified three high N(H I) absorbers present in at least one of the two lines of sight at redshifts $z_{\rm abs} = 2.47$ (B only), 2.66 (A and B) and 2.94 (A and B).

2.2 Column density determination

The H I column densities of the absorbers at $z_{\rm abs} = 2.47$, 2.66 and 2.94 were determined by fitting the continuum normalized spectra with damped profiles using the DIPSO software. The fits to the data are shown in Figs 2–4. For all five absorbers, we detect metal lines, including Si II, Fe II, S II, Zn II and Ni II, see Figs 5–7. Since the resolution of ESI is significantly larger than the Doppler widths of the metal lines, Voigt component fitting does not yield a physically meaningful decomposition of the line profile. Instead, column densities are determined using the apparent optical depth method (AODM; e.g. Savage & Sembach 1991). Accurate column densities of typically weak lines such as Zn II can be well determined in lower resolution spectra. For example, the early work of Pettini et al. (1997) determined N(Zn II) from spectra with FWHM ∼ 1 Å, similar to ESI's resolution, which have subsequently been confirmed with higher resolution echelle spectroscopy. The AODM also allows us to assess the impact of saturation in unresolved lines when multiple transitions from a given species are observed. This is often the case for Fe II lines, and when saturation is suspected, we adopt the maximum column density, usually derived from the weakest transition. The main disadvantage of the AODM is that the assessment of contamination and blending is less straightforward.

Due to their ionization potentials, it is usually assumed that the singly ionized species represent the dominant state of elements in DLAs. For absorbers with log N(H I) $\gtrsim$ 20.0 there may be a

[1] http://www2.keck.hawaii.edu/inst/esi/ESIRedux/index.html
[2] http://star-www.rl.ac.uk/star/dvi/sun50.htx/sun50.html

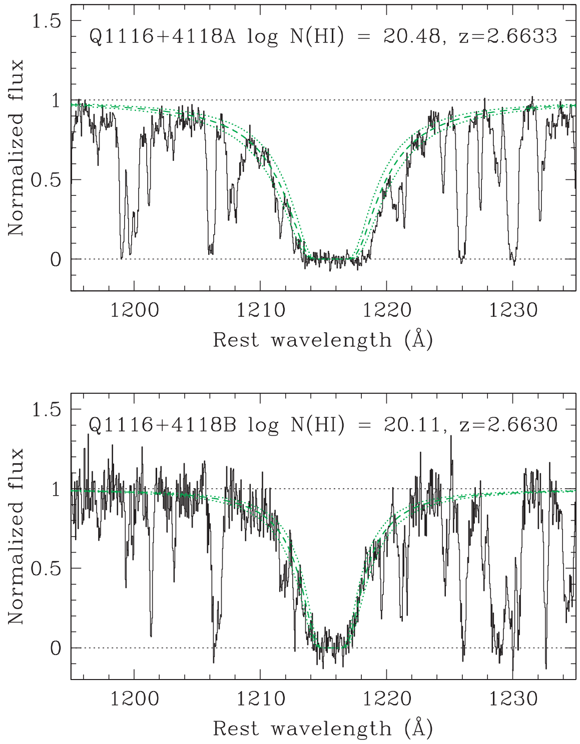

Figure 3. Lyα fit (dashed profile) and error (dotted profiles) to the $z_{abs} \sim 2.66$ DLA/sub-DLA seen towards QSO A (top panel) and QSO B (bottom panel). The transverse separation of the two sightlines at this redshift is 110 h_{70}^{-1} kpc.

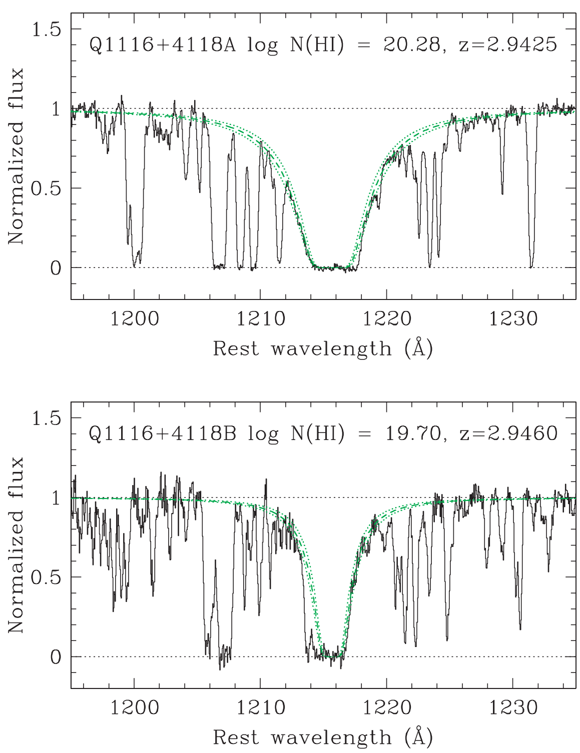

Figure 4. Lyα fit (dashed profile) and error (dotted profiles) to the $z_{abs} \sim 2.94$ DLA/sub-DLA seen towards QSO A (top panel) and QSO B (bottom panel). The transverse separation of the two sightlines at this redshift is 107 h_{70}^{-1} kpc.

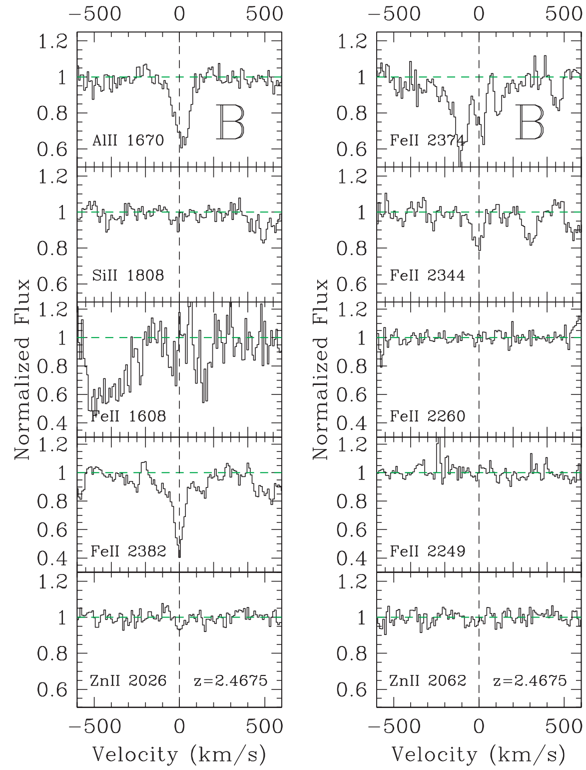

Figure 5. Metal lines for the sub-DLA detected towards QSO B at $z_{abs} \sim 2.4677$.

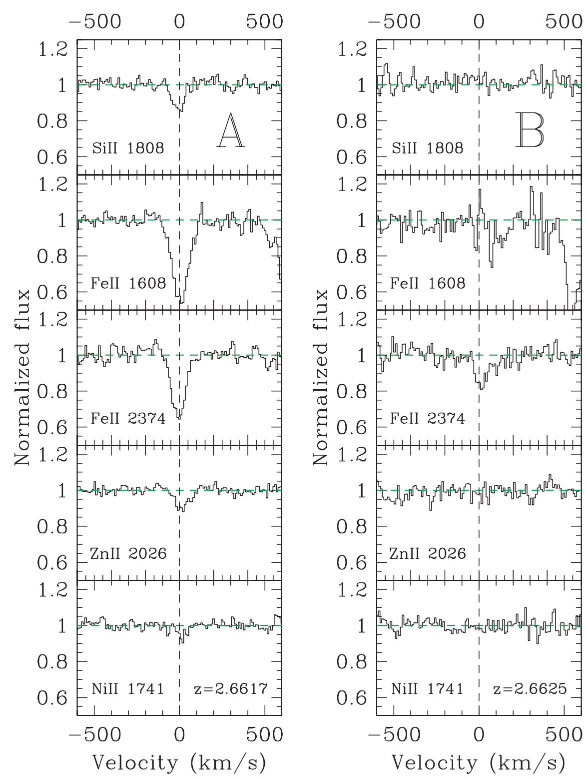

Figure 6. A selection of detected metals for the DLA/sub-DLA detected towards QSO A (left-hand column) and QSO B (right-hand column) at $z_{abs} \sim 2.66$. The *x*-axis shows a velocity scale relative to the centre of the metal line absorption, whose redshift is given in the bottom panels.

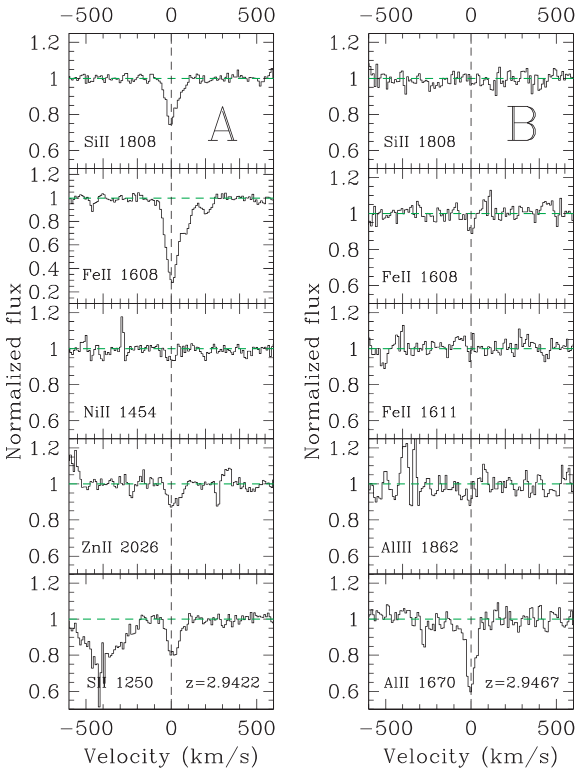

Figure 7. A selection of detected metals for the DLA/sub-DLA detected towards QSO A (left-hand column) and QSO B (right-hand column) at $z_{\rm abs} \sim 2.94$. The *x*-axis shows a velocity scale relative to the centre of the metal line absorption, whose redshift is given in the bottom panels.

non-negligible ionization correction which undermines this assumption. When a range of metal lines from different ionization states are detected, it is possible to model their relative contributions. Often this can be done with Al II plus Al III or Fe II plus Fe III. However, as described below, for the two absorbers in our spectra with log N(H I) < 20.0 such an estimate of ionization correction is not possible due to the limited number of transitions that we detect. In our abundance determinations we therefore assume that N(X) = N(X II) when log N(H I) > 20.0, but for the lower N(H I) absorbers we quote only column densities and not abundances.

Fits to both H I and metal line species are now described in the following subsections on an absorber-by-absorber basis. The redshifts that we allocate to each absorber refer to zero velocity for the metal lines, not the value determined from the Lyα.

2.2.1 $z_{\rm abs} = 2.4675$ sub-DLA towards QSO B

Despite the low N(H I) of this absorber and the relatively poor S/N in the blue part of QSO B's spectrum, clear damping wings allow us to constrain the hydrogen column density to within 0.15 dex (not including continuum fit errors). No corresponding DLA or sub-DLA is seen towards QSO A, although there is a saturated Lyα absorber at $z_{\rm abs} = 2.4688$ corresponding to a velocity offset of $\Delta v = 95$ km s^{-1} from the best-fitting H I redshift of $z_{\rm abs} = 2.4677$.

Although the low N(H I) and relatively poor S/N preclude the detection of many metal line species, we do detect several lines of Fe II (although many are blended) as well as Al II λ 1670 and Zn II λ 2026, see Table 2. We adopt the Fe II column density from the

Table 2. Ionic column densities for $z_{\rm abs} = 2.4675$ sub-DLA towards QSO B.

Ion	λ	f-value	log N	log $N_{\rm adopt}$
H I	1215.6701	0.416 40		19.85 ± 0.15
Al II	1670.7874	1.880	12.73 ± 0.09	12.73 ± 0.09
Fe II	1608.4511	0.0580	<13.6	13.33 ± 0.12
Fe II	2260.7805	0.002 44	<14.2	
Fe II	2249.8768	0.001 821	<14.4	
Fe II	2344.2140	0.1140	13.33 ± 0.12	
Fe II	2374.4612	0.0313	14.10 ± 0.09	
Fe II	2382.7650	0.3200	13.42 ± 0.07	
Si II	1808.0130	0.002 186	<14.4	<14.4
Zn II	2026.1360	0.4890	12.08 ± 0.26	<12.3
Zn II	2062.6640	0.2560	<12.3	
Cr II	2056.2539	0.1050	<12.6	<12.6

All limits are 3σ.

2344 Å line since the other detected transitions of this species (Fe II $\lambda\lambda$ 2374, 2382) are blended (see Fig. 5).

One potentially serious problem with lower resolution data is blending either with species at the same wavelength (e.g. Zn II λ 2062 with Cr II λ 2062) or from lines at other redshifts. At high resolution, this is usually easily identified during the Voigt profile fitting process, but is not always obvious in lower dispersion data. This issue is relevant in our determination of a Zn II column density, since the Zn II λ 2026 line [the stronger of the two ultraviolet (UV) lines] is only separated from Mg I λ 2026 by 50 km s^{-1}. The relative strengths of Mg I and Zn II will depend on a variety of factors, including intrinsic abundance ratios, differential dust depletion and ionization structure of the absorber. For DLAs and sub-DLAs with high column densities of metals, it seems that Mg I can contribute significantly to the total EW at $\lambda \sim 2026$ (e.g. Herbert-Fort et al. 2006; Péroux et al. 2006; York et al. 2006). Although this is unlikely to be a serious problem for this sub-DLA, whose metal column densities are not large, we conservatively quote an upper limit for N(Zn II) based on the non-detection of Zn II λ 2062. Without a correction for Mg I and without an ionization correction (see below) the Zn abundance determined from Zn II λ 2026 is high, about 0.4 $Z_{\odot}$. It would therefore be very interesting to improve the S/N for this absorber to confirm (or otherwise) this relatively high metallicity. With the limited metal column densities we are able to reliably measure, it is not possible to determine ionization corrections for this absorber, so we do not attempt to convert our AODM measurements into abundances.

It is interesting to note that although the extent of C IV galaxy haloes are usually considered to have large sizes (up to a few hundred kpc, Steidel 1995; Adelberger et al. 2005b), in this case, there is a C IV absorber in QSO A at $z_{\rm abs} = 2.4532$ compared with a redshift for C IV in QSO B (where the sub-DLA is detected) of $z_{\rm abs} = 2.4683$. This corresponds to a velocity difference of ~1300 km s^{-1}. It is not clear whether the C IV absorption in QSO A is associated with the sub-DLA detected in QSO B. The interpretation of C IV halo sizes clearly depends on the velocity tolerance permitted for line matches. We will analyse the C IV absorbers in this pair, and a larger sample, in a forthcoming paper.

2.2.2 $z_{\rm abs} = 2.6617$ DLA towards QSO A and $z_{\rm abs} = 2.6625$ sub-DLA towards QSO B

For the DLA towards QSO A we detect metal lines from the following species: Fe II, Si II, Zn II, Al III and Ni II and determine an upper

Table 3. Ionic column densities for $z_{abs} = 2.6617$ DLA towards QSO A.

Ion	λ	f-value	$\log N$	$\log N_{adopt}$
H I	1215.6701	0.416 40		20.48 ± 0.10
Al III	1854.7164	0.5390	12.97 ± 0.10	12.97 ± 0.10
Al III	1862.7895	0.2680	12.99 ± 0.14	
Fe II	1608.4511	0.0580	14.41 ± 0.05	14.36 ± 0.10
Fe II	1611.2005	0.001 360	<14.5	
Fe II	2344.2140	0.1140	14.22 ± 0.03	
Fe II	2374.4612	0.0313	14.30 ± 0.06	
Fe II	2382.7650	0.3200	14.12 ± 0.03	
Si II	1808.0130	0.002 186	15.05 ± 0.11	15.05 ± 0.11
Zn II	2026.1360	0.4890	12.60 ± 0.13	12.40 ± 0.20
Zn II	2062.6640	0.2560	12.40 ± 0.20	
Cr II	2056.2539	0.1050	<12.7	<12.7
Ni II	1741.5531	0.042 70	13.35 ± 0.20	13.35 ± 0.20

All limits are 3σ.

limit for Cr II, see Table 3 and Fig. 6. We also detect Al II λ 1670, but this transition is blended with C IV at $z_{abs} \sim 2.94$ so we do not quote a column density for it. For the Fe II column density, we adopt an average of the $\lambda\lambda$ 1608 and 2374 transitions which are the least likely to suffer from saturation.

As mentioned in the previous subsection, Mg I may be a significant contaminant at 2026 Å. The most common way to calculate the contribution from Mg I is to measure N(Mg I) from the Mg I λ 2852 line and predict the contribution at 2026 Å according to the relative oscillator strengths. However, at a redshift of $z_{abs} \sim 2.66$ the Mg I λ 2852 line is shifted into the infrared. We therefore rely on Zn II λ 2062 to provide a Zn II column density. Although the Zn II λ 2062 Å line can itself suffer from blending with Cr II λ 2062, in this case the upper limit on the stronger Cr II λ 2056 rules out this possibility. Comparing the column densities derived from the two Zn II lines in Table 3 shows that the contribution from Mg I at λ 2026 would have led to an overestimate of N(Zn II) by ~0.2 dex.

For the sub-DLA towards QSO B, we only determine a column density for Fe II (see Table 4) since Al III $\lambda\lambda$ 1854, 1862 have very broad profiles and are slightly offset from the central velocity, so may be blends or misidentifications. The usually strong Al II λ 1670 is also in a blended part of the spectrum.

2.2.3 $z_{abs} = 2.9422$ *sub-DLA towards QSO A and* $z_{abs} = 2.9467$ *sub-DLA towards QSO B*

The best-fitting N(H I) to the $z_{abs} \sim 2.94$ absorber in QSO A yields a column density just below the DLA threshold, although within the error bars it may still be a 'classical' DLA. The absorber towards QSO B appears to be a blend, but the red damping wing allows a reasonable H I fit that classifies this absorber as a sub-DLA.

Table 4. Ionic column densities for $z_{abs} = 2.6625$ sub-DLA towards QSO B.

Ion	λ	f-value	$\log N$	$\log N_{adopt}$
H I	1215.6701	0.416 40		20.11 ± 0.10
Fe II	2344.2140	0.1140	13.54 ± 0.09	13.87 ± 0.13
Fe II	2374.4612	0.0313	13.87 ± 0.13	
Si II	1808.0130	0.002 186	<14.4	<14.4
Zn II	2026.1360	0.4890	<12.1	<12.1
Cr II	2056.2539	0.1050	<12.7	<12.7
Ni II	1741.5531	0.042 70	<13.0	<13.0

All limits are 3σ.

Table 5. Ionic column densities for $z_{abs} = 2.9422$ sub-DLA towards QSO A.

Ion	λ	f-value	$\log N$	$\log N_{adopt}$
H I	1215.6701	0.416 40		20.28 ± 0.05
S II	1250.5840	0.005 453	15.01 ± 0.10	15.01 ± 0.10
S II	1253.8110	0.010 88	15.01 ± 0.08	
Al II	1670.7874	1.880	13.84 ± 0.06	$\geqslant 13.84$
Al IIIl	1854.7164	0.5390	13.73 ± 0.04	$\geqslant 13.73$
Al III	1862.7895	0.2680	13.73 ± 0.07	
Fe II	1608.4511	0.0580	14.69 ± 0.04	14.69 ± 0.04
Fe II	1611.2005	0.001 360	14.66 ± 0.21	
Si II	1808.0130	0.002 186	15.34 ± 0.08	15.34 ± 0.08
Zn II	2026.1360	0.4890	12.62 ± 0.12	12.40 ± 0.33
Ni II	1370.1310	0.076 90	13.71 ± 0.23	13.66 ± 0.28
Ni II	1454.842	0.0323	13.60 ± 0.21	

All limits are 3σ.

For the $z_{abs} = 2.9422$ sub-DLA towards QSO A we detect a range of metal species: Si II, Fe II, Zn II, S II, Ni II, Al II and Al III, see Table 5 and Fig. 7. N V λ 1242 may be present, but is weak (peak optical depth $\tau \sim 0.1$) and blended with another feature. We do not quote a detection or limit for Cr II since all the lines are in a contaminated part of the spectrum. Al II λ 1670 is clearly saturated, so we only quote a lower limit for N(Al II). For Al III $\lambda\lambda$ 1854, 1862 the two lines give consistent column densities, despite their high EWs. However, to be cautious, we quote their column densities as lower limits. The Fe II λ 1608 line towards QSO A is quite strong and may be slightly saturated. However, the much weaker Fe II λ 1611 is marginally detected and gives a consistent column density.

We have the same problem for Zn II as for the DLA at $z_{abs} \sim 2.66$ discussed in the previous subsection, that is, the potential contribution from Mg I to the Zn II λ 2026 line. However, the situation is even more complicated in this case because not only is Mg I λ 2852 not covered, but also the Zn II λ 2062 line is in a highly contaminated part of the spectrum, so cannot be used and we have no estimate of the Cr II contribution. We therefore estimate an upper limit to the contribution of Mg I by considering values measured in other metal-rich absorbers. From Péroux et al. (2006) and Herbert-Fort et al. (2006), we assume a rest-frame upper limit contribution of 50 mÅ from Mg I. This means that N(Zn II) may require a downward revision of up to 0.4 dex. We therefore quote a column density of Zn II with error bars that account for this range of possibilities, see Table 5. Regardless of our uncertainties in N(Zn), this absorber is clearly metal-rich, since the column densities of Si and S also yield abundances $\sim 1/3\,Z_{\odot}$.

We also search for H_2 in the sub-DLA towards QSO A. At $z_{abs} = 2.9422$ we have coverage of Lyman $J = 0$, 1 rotational bands for 6–0 to 0–0 vibrational transitions. These first two J states usually dominate the molecular column density in DLAs (e.g. Ledoux, Petitjean & Srianand 2003). Assuming a redshift matched to the central position of the metal lines, that is, $z_{abs} = 2.9422$, we combine the limits on $J = 0$ and 1 to determine a limit of $\log N(H_2) < 14.5$ in this line of sight.

For the sub-DLA towards QSO B, we only determine column densities for Fe II and Al II and upper limits for the other species listed in Table 6. Al III λ 1854 is in a region of moderate contamination in the B spectrum, so that the column of a weak line is unreliable. There is a marginally significant (2.6σ) feature close to the expected

Table 6. Ionic column densities for $z_{abs} = 2.9467$ sub-DLA towards QSO B.

Ion	λ	f-value	$\log N$	$\log N_{adopt}$
H I	1215.6701	0.416 40		19.70 ± 0.10
S II	1253.8110	0.010 88	<14.0	<14.0
Al II	1670.7874	1.880	12.57 ± 0.10	12.57 ± 0.10
Al III	1862.7895	0.2680	12.51 ± 0.22	<12.6
Fe II	1608.4511	0.0580	13.29 ± 0.25	13.29 ± 0.25
Si II	1808.0130	0.002 186	<14.6	<14.6
Zn II	2026.1360	0.4890	<12.1	<12.1
Ni II	1370.1310	0.076 90	<13.4	<13.4

All limits are 3σ.

position of Al III λ 1862, but since it is below the 3σ level, we quote it as a limit.

3 DISCUSSION

3.1 Abundances

The final abundances for the three absorbers with $\log N(\mathrm{H\,I}) > 20$ are given in Table 7. The two absorbers in QSO A both have very high metallicities, based on the abundance of Zn: 1/3 and 1/5 $\mathrm{Z}_\odot$. Such high metallicities are very rare even in low-redshift DLAs (e.g. Meiring et al. 2006), leading to the widespread conclusion that the DLA cross-section is dominated by metal-poor gas. It has been suggested that this may be due to a dust-induced bias against metal-rich galaxies, although there is currently no observational evidence to support this claim (e.g. Ellison et al. 2001, 2004a; Akerman et al. 2005; Ellison, Hall & Lira 2005a; Jorgenson et al. 2006). Herbert-Fort et al. (2006) have shown that selecting absorbers from the SDSS on the basis of strong metal lines can readily identify DLAs with metallicities in excess of 0.1 $\mathrm{Z}_\odot$, indicating that metal-rich systems do exist at high redshift, but are simply rare. The two DLAs studied here have metallicities consistent with the metal-strong population of Herbert-Fort et al. (2006). Moreover, the abundances that we determine are comparable to those measured in cB58 (2/5 $\mathrm{Z}_\odot$ at $z = 2.7$, Pettini et al. 2002) and other LBGs at $2 < z < 3$ (Teplitz et al. 2000; Shapley et al. 2004).

We also determine relatively high depletion factors for the DLAs based on [Zn/Fe] = +0.88, +0.55 in the DLAs at $z_{abs} = 2.66$ and 2.94, respectively. These values are usually considered as measures of the dust-to-metals ratio, since these two elements trace each other well in most Galactic stars (although see the caveats in Nissen et al. 2004), yet Fe is highly refractory whereas Zn is not (Savage & Sembach 1996). The relative abundances measured here imply that ~15–30 per cent of the metals in these two DLAs are in the gas phase and follows the broad trend of increased depletion with increasing metallicity (e.g. Meiring et al. 2006 for the most recent compilation). Although quite extreme by DLA standards, these depletion factors still barely overlap with measurements in the Galactic disc and Magellanic Clouds (e.g. Roth & Blades 1997).

Although this sightline intersects gas associated with the diffuse ISM, given its high metallicity (1/3 $\mathrm{Z}_\odot$) and high depletion, it is perhaps surprising that we do not detect H_2 down to a molecular fraction of $\log f(\mathrm{H_2}) = 2N(\mathrm{H_2})/[2N(\mathrm{H_2}) + N(\mathrm{H\,I})] < -5.5$ for the $z_{abs} = 2.94$ DLA.[3] Ledoux et al. (2003) and Petitjean et al. (2006) have suggested that both metallicity and depletion may be important factors for a galaxy to be able to form (and maintain) a significant column density of molecules. As a comparison with the $z_{abs} = 2.94$ DLA studied here, we can consider molecular fractions in Large Magellanic Cloud (LMC) sightlines, where the metallicity is similar to this DLA. Tumlinson et al. (2002) showed that H_2 is detected in ~50 per cent of LMC sightlines, so we may naively expect a similar detection rate in other galaxies with similar metallicities. Although the statistics for metal-rich DLAs are still poor, a 50 per cent detection rate does broadly fit the high-redshift data for DLAs with metallicities above 1/5 $\mathrm{Z}_\odot$ (Petitjean et al. 2006). However, metallicity is clearly not the only factor, since the Small Magellanic Cloud, whose metallicity is a factor of 3 lower than the LMC, has detections for 90 per cent of the sightlines studied by Tumlinson et al. (2002). This has been proposed to be due to higher star formation rates in the LMC which preferentially photodissociate molecules.

Finally, we note that the $z_{abs} = 2.94$ DLA has a relative abundance of S and Zn that is close to the solar value, [S/Zn] = +0.05. In Galactic stars, we observe enhanced α/Fe ratios at metallicities below [Fe/H] < −1.0, due to the time delay between supernovae of type II (SNII) and type Ia (SNIa) enrichment. In DLAs, the two undepleted elements S (an α element) and Zn (which traces the Fe peak in Galactic halo stars at [Fe/H] > −2.5) are usually preferred tracers of the relative contributions of SNIa and SNII (e.g. Nissen et al. 2004). The universally low (typically subsolar) values of [S/Zn] in DLAs indicate that their chemical enrichment history is very different to that of the Milky Way. New measurements from local dwarf galaxies indicate that low α/Fe ratios may actually be common in the Local Group, for example, Shetrone et al. (2003). At a metallicity of 1/3 $\mathrm{Z}_\odot$ the value of [S/Zn] measured here is actually intermediate between typical Galactic values (e.g. Gratton et al. 2003) and those found in the more metal-rich Local Group dwarfs such as Fornax, the LMC and Sagittarius (Bonifacio et al. 2004; Pompéia, Hill & Spite 2005).

3.2 Are DLA galaxies over 100 h_{70}^{-1} kpc in size?

At low redshift, we have a number of measurements of DLA absorber size. At $z = 0$, Zwaan et al. (2005) showed that a 21-cm survey of selected UGC galaxies finds typical dimensions for DLA-equivalent column densities ranging from ~5–50 kpc, depending on galaxy mass and orientation. At similarly low redshifts ($cz < 4000$ km s^{-1}) Bowen, Pettini & Blades (2002) found that if a line of sight passes within 200 kpc of a nearby galaxy, the covering factor for H I gas with $\log N(\mathrm{H\,I}) > 13$ is effectively 100 per cent. However, the cross-section of gas that is optically thick at the Lyman limit will be considerably smaller than for absorbers with $13 < \log N(\mathrm{H\,I}) < 16$. At these lower column densities, the H I absorption can presumably be associated not only with extended, diffuse haloes, but also with non-Galactic structures such as filaments and intragroup media. At intermediate redshifts, Chen & Lanzetta (2003) determined a characteristic size for DLAs of $R_\star \sim 25$ kpc, and also found that a significant number of DLA fields have multiple galaxies at the absorber redshift. In contrast, constraints on galaxy/absorber size on kpc scales at $z > 2$ are very few. They are limited to two pairs of QSO sightlines which probe transverse scales of 5–10 kpc (Smette et al. 1995; Lopez et al. 2005), a measurement of spatially offset Lyα fluorescence (Adelberger et al. 2006), a handful of extended radio sources (Foltz et al. 1988; Briggs et al. 1989) and extended [O III] emission from three DLAs at $2 < z < 3$ (Møller et al. 2004; Weatherley et al. 2005). Although these observations

[3] Although it is possible that we have underestimated the contribution of Mg I to the Zn II λ 2026 line and the true metallicity may be less than we have deduced. However, the abundance based on Si or S is also 1/3 $\mathrm{Z}_\odot$.

Table 7. Abundances for absorbers with N(H I) > 20.1.

QSO	z_{abs}	log N(H I)	[Fe/H]	[Si/H]	[Zn/H]	[Cr/H]	[S/H]	[Ni/H]
A	2.6617	20.48 ± 0.10	-1.59 ± 0.14	-0.97 ± 0.15	-0.71 ± 0.22	< -1.43	–	-1.35 ± 0.22
B	2.6625	20.11 ± 0.10	-1.71 ± 0.16	< -1.25	< -0.51	< -1.06	–	< -1.33
A	2.9422	20.28 ± 0.05	-1.06 ± 0.06	-0.48 ± 0.09	-0.51 ± 0.33	–	-0.46 ± 0.11	-0.84 ± 0.28

All limits are 3σ.

generally imply gaseous extents of at most a few tens of kpc, Labbé et al. (2003) have used deep imaging to detect a population of galaxies at $1.5 < z < 3$ whose discs have a comparable size to the Milky Way and Prochaska & Wolfe (1997) have also interpreted DLAs as large discs. The critical question is therefore: is it likely that the common absorption seen in SDSS 1116+4118 AB is due to galaxies with 100 kpc gas haloes at $z \sim 3$?

Some first clues as to whether the coincident absorption is due to a common structure can be gleaned from the relative velocities across the line of sight. Based on the metal lines, the velocity separations between the DLA/sub-DLA in QSO A/B are 65 km s^{-1} ($z_{abs} \sim 2.66$) and 340 km s^{-1} ($z_{abs} \sim 2.94$). Although only a handful of rotation curves and velocity fields have been studied at high redshift (e.g. Erb et al. 2003, 2004), a significant number have velocity dispersions in excess of 200 km s^{-1} and rotation velocities >150 km s^{-1} (i.e. a total velocity difference >300 km s^{-1}). Therefore, although the shear between QSO A and B is large for the $z_{abs} \sim 2.94$ absorber, it is still feasible that it is within the same galaxy.

We can also appeal to the metallicities for clues to the absorbers' structure. At both $z \sim 2.66$ and $\sim$2.94, at least one of the absorbers has a high metallicity. On the one hand, the existence of a mass–metallicity relation at all redshifts studied (Tremonti et al. 2004; Erb et al. 2006; Savaglio et al. 2005) indicates that these galaxies may have stellar masses at least $\sim 10^9$–$10^{9.5}$ M$_{\odot}$, possibly lending support to the idea of a large physical extent. On the other hand, such high abundances seen in absorption, consistent with metallicities inferred from the emission-line measurements in LBGs, indicates that these sightlines may intersect the central part of their galaxies. If true, it would imply even larger sizes for the absorbing galaxy than the simple interpretation of common coincidence, that is, $r \gtrsim 100\,h_{70}^{-1}$ kpc, rather than $d \gtrsim 100\,h_{70}^{-1}$ kpc. However, the information on neither metallicity nor velocity provides very satisfactory conclusions as to the nature of the coincident absorption. We therefore turn to galaxy simulations to help us interpret our observations.

3.2.1 *Cosmological simulations of galaxy formation*

The code used for the simulations is a significantly improved version of the TreeSPH code, which has been used previously for galaxy formation simulations (Sommer-Larsen, Götz & Portinari 2003). The main improvements over the previous version are as follows. (1) The 'conservative' entropy equation solving scheme (Springel & Hernquist 2002). (2) Non-instantaneous gas recycling and chemical evolution, tracing 10 elements (Lia, Portinari & Carraro 2002a,b); the algorithm includes SNII and SNIa, and mass-loss from stars of all masses. (3) Atomic radiative cooling depending both on the metal abundance of the gas and on the metagalactic UV field, modelled after Haardt & Madau (1996) is invoked, as well as simplified treatment of radiative transfer, switching off the UV field where the gas becomes optically thick to Lyman-limit photons on scales of $\sim$1 kpc.

In this paper, very high-resolution simulations of two galaxies, known to become large disc galaxies at $z = 0$, are analysed in relation to DLA and sub-DLA sightline properties. We take the two galaxies simulated by Razoumov & Sommer-Larsen (2006), K15 and K33, which have, at $z = 0$, characteristic circular speeds of $V_c = 245$ and 180 km s^{-1}, respectively. The galaxies bracket typical disc galaxy formation histories: the formation of the larger K15 disc is merger induced (e.g. also Robertson et al. 2004), with the disc growing strongly between $z = 1$ and 0, whereas K33 already starts developing a disc by $z \sim 2.5$, which subsequently grows gradually to the present epoch. The $z = 0$ virial masses of the two galaxies are $M_{vir} = 8.9 \times 10^{11}$ and 3.7×10^{11} M$_{\odot}$, for K15 and K33, respectively.

The two galaxies were simulated in the standard ΛCDM cosmology using the 'zoom-in' technique (e.g. Sommer-Larsen 2006) to study the formation and evolution of individual galaxies in full cosmological context. Total particle numbers used were 2.2 and 1.2 million, for K15 and K33, respectively. Particle masses and gravitational (spline) softening lengths of $m_{gas} = m_* = 8.45 \times 10^4$ and $m_{DM} = 4.83 \times 10^5\,h_{70}^{-1}$ M$_{\odot}$, and $\epsilon_{gas} = \epsilon_* = 176$ and $\epsilon_{DM} = 316\,h_{70}^{-1}$ pc, respectively, were adopted. The gravity softening lengths were fixed in physical coordinates from $z = 6$ to 0, and in comoving coordinates at earlier times. The minimum SPH smoothing length in the simulation was about $12\,h_{70}^{-1}$ pc. A Kroupa initial mass function (Kroupa 1998) was used in the simulations, and early rapid and self-propagating star formation (sometimes dubbed 'positive feedback') was invoked (Sommer-Larsen et al. 2003).

Although K15 and K33 galaxies have been chosen from our simulation to represent two different disc galaxy evolutionary paths (and end products) there are some generic features to both galaxies. For example, they both tend to be larger and have a more extended gas distribution at higher redshift. At low redshift, the gas has cooled and settled into a more organized and centrally concentrated structure. However, protodiscs can form even at quite high redshifts (see the top left-hand panel of Figs 8 and 9). The two different scales for these figures highlight that the majority of DLA gas is distributed on scales of tens, rather than hundreds, of kpc. Moreover, the region of the galaxy which is actively star forming is very small ($\sim$ kpc scale) compared with the distribution of high column density gas. This is qualitatively consistent with the observation of low abundances in DLAs (e.g. Pettini et al. 1999) compared with emission-line abundances in absorption-selected galaxies (e.g. Chen, Kennicutt & Rauch 2005; Ellison, Kewley & Mallén-Ornelas 2005b). The spatial separation of the bulk of DLA-inducing gas from the regions of high star formation has also been inferred by the lack of low surface brightness galaxies in the *Hubble Ultra-Deep Field* (Wolfe & Chen 2006).

We analyse the model galaxies by passing sightlines through the simulation box and integrating the H I volume density along the line of sight. In Figs 8–10 we show two projections of the two simulated galaxies where each box has been projected into a 600×600 grid. The colour contours show the projected H I gas column density in units of atoms cm^{-2} and are therefore analogous to the

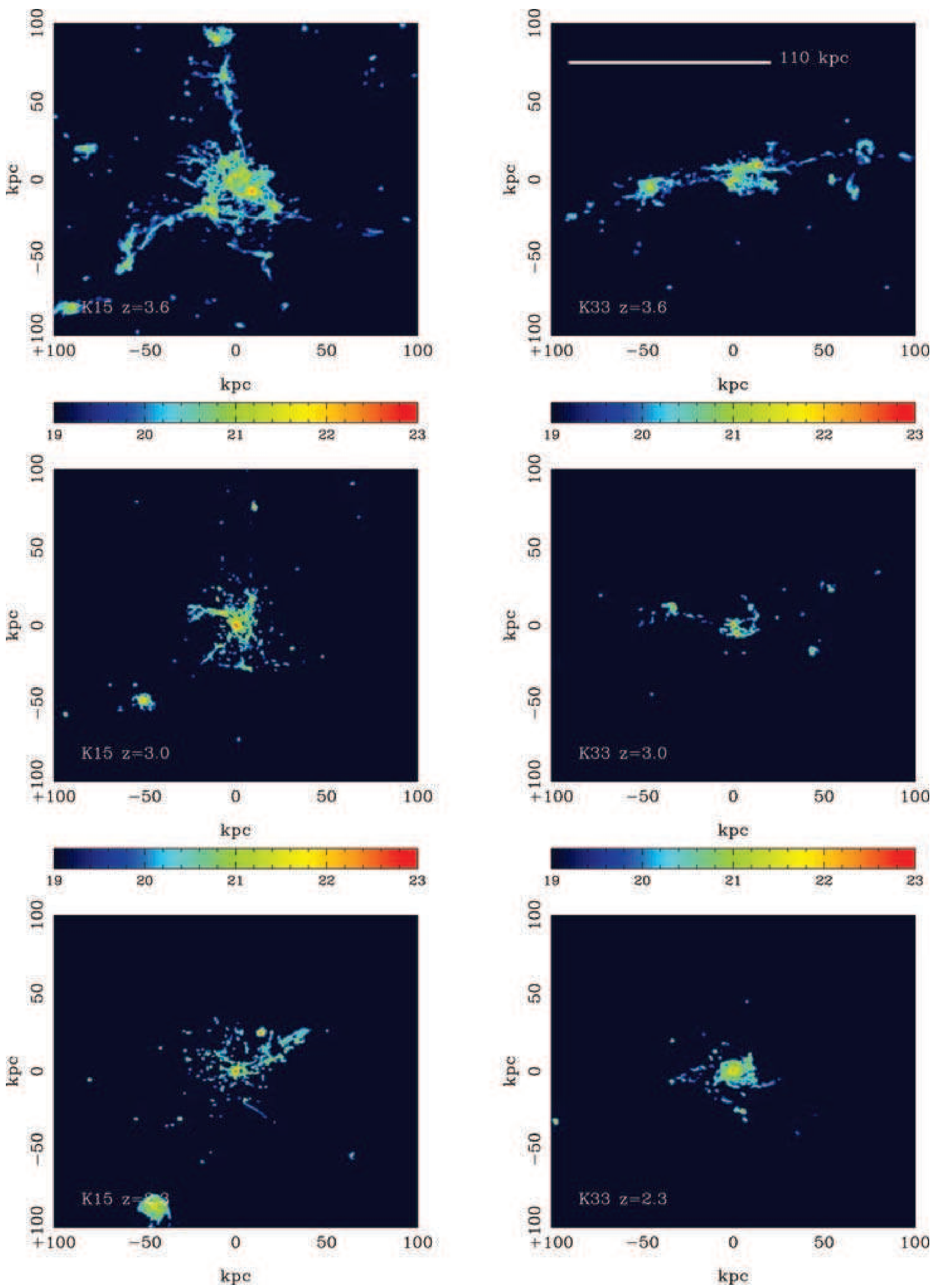

Figure 8. Projected N(H I) map for the central 200 kpc for our two simulated galaxies, K15 (left-hand panel) and K33 (right-hand panel) at $z = 3.6, 3.0$ and 2.3 (top through bottom panels). This projection is through the *XY* (face-on) plane. The bar in the top right-hand panel shows the typical transverse separation at the absorber radshift for the QSO pair studied here. The white bar in the top right-hand panel shows 110 h_{70}^{-1} kpc, the approximate physical separation of the two lines of sight at the absorbers' redshift in SDSS1116+4118 AB.

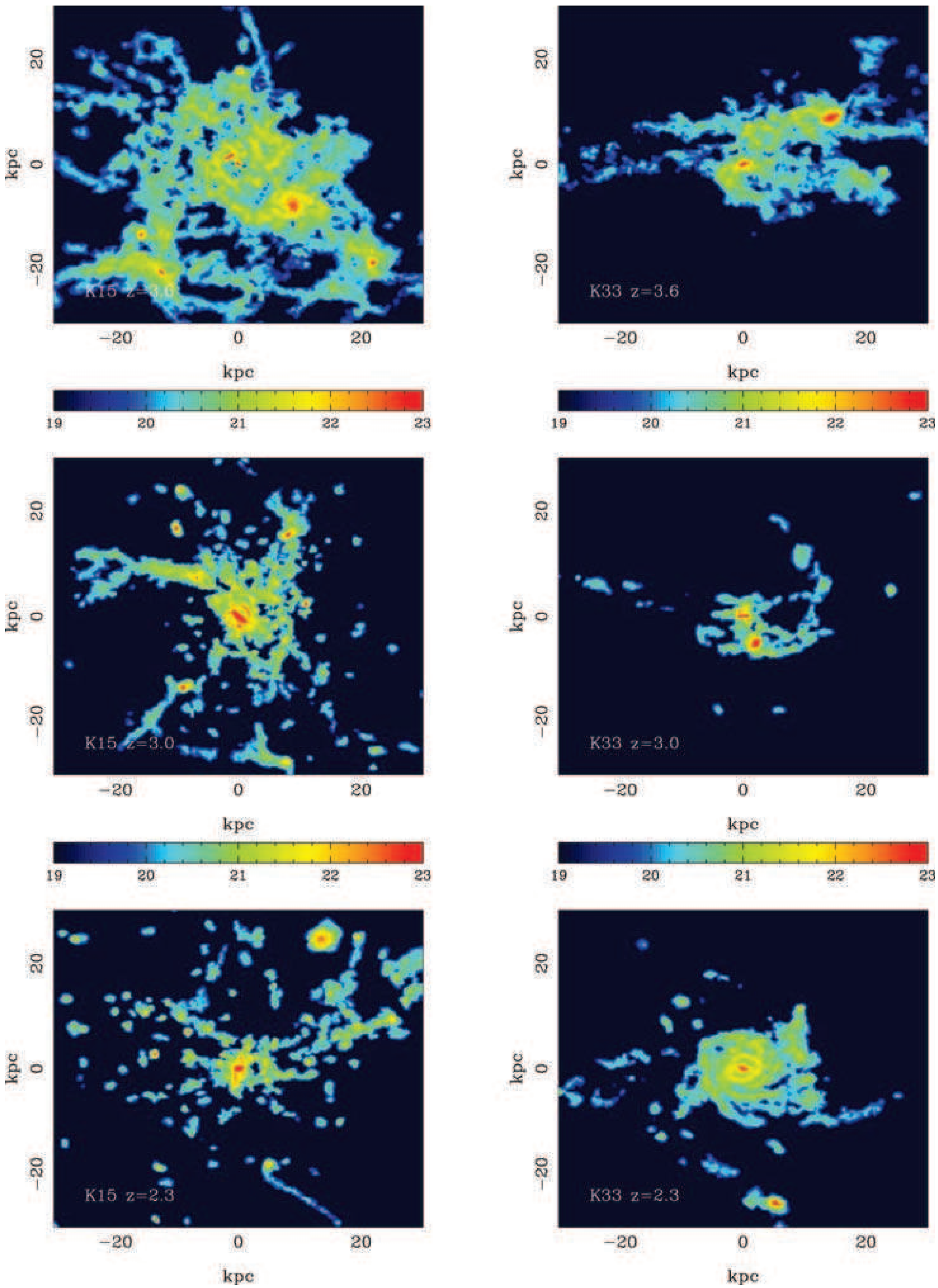

Figure 9. Projected N(H I) map for the central 60 kpc for our two simulated galaxies, K15 (left-hand panel) and K33 (right-hand panel) at $z = 3.6$, 3.0 and 2.3 (top through bottom panels). This projection is through the XY (face-on) plane.

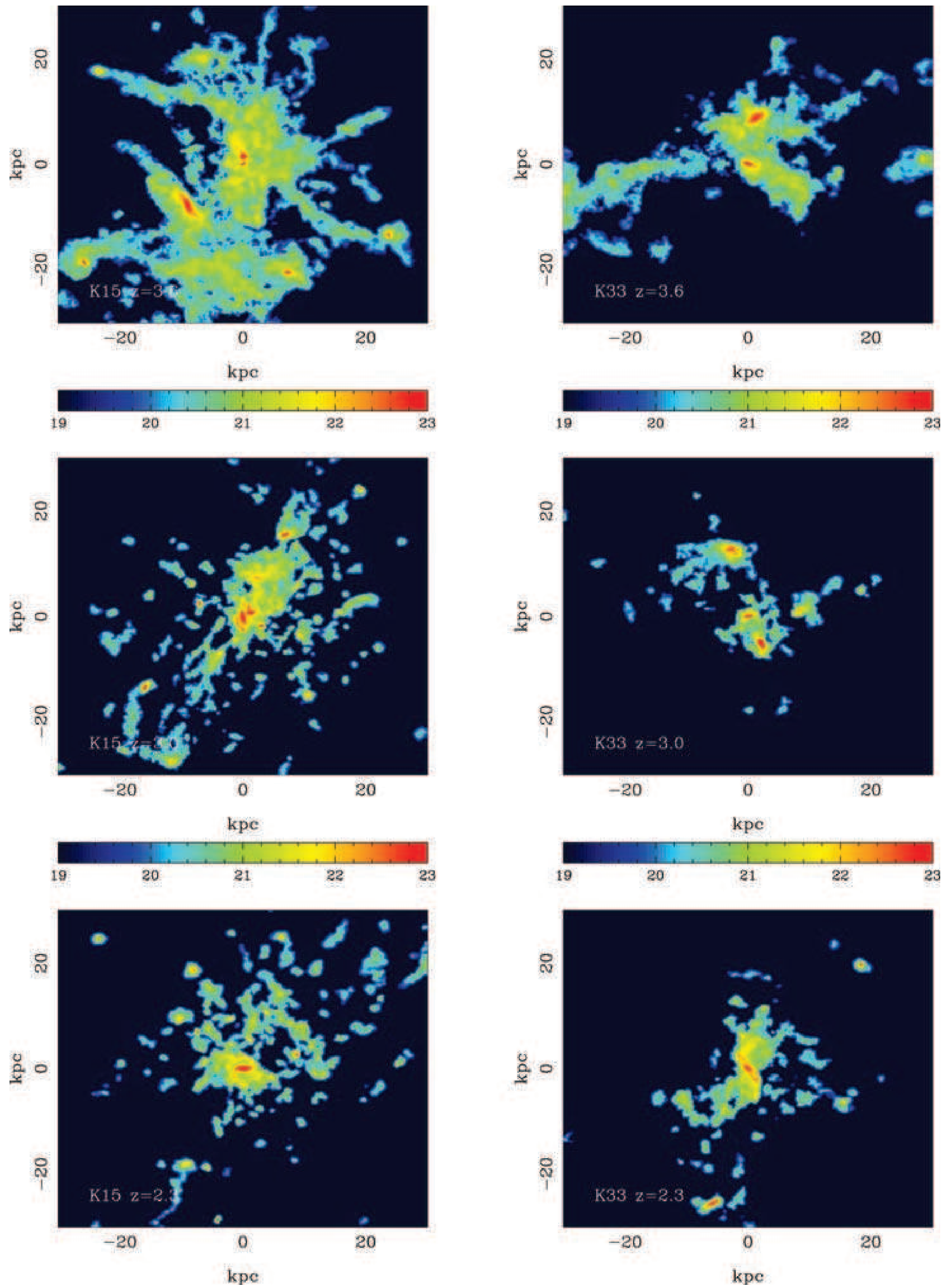

Figure 10. Projected N(H I) map for the central 60 kpc for our two simulated galaxies, K15 (left-hand panel) and K33 (right-hand panel) at $z = 3.6, 3.0$ and 2.3 (top through bottom panels). This projection is through the *XZ* (edge-on) plane.

observed N(H I) columns measured in QSO sightlines. The N(H I) at each point along the line of sight is evaluated by weighting all of the particles within the local smoothing length h (where $2h$ is the distance within which 50 particles are located) according to the spline smoothing kernel (Monaghan & Lattanzio 1985). For this work, we use two different renderings of each galaxy in order to alleviate orientation effects. These two projections correspond to projecting lines of sight through the XY and XZ faces of the same simulation cube. The XY plane corresponds roughly to a face-on configuration of the central star-forming disc whereas the XZ is approximately edge-on. However, as can be seen from a visual inspection of Figs 8–10, the distribution of H I gas is not significantly different even in these two 'extreme' orientations; this is checked quantitatively below. Although we do not use simulations at lower redshifts, for demonstration purposes we include here images of the K33 at $z = 0.3$, the lowest redshift to which the simulation has currently progressed. Fig. 11 shows the galaxy on two spatial scales and in both the face-on and edge-on orientations. These images show the stability and growth of the disc since $z = 3.6$. The K15 simulation has not yet progressed beyond $z = 2.0$, so we cannot show a lower redshift rendition.

In order to calculate the probability of finding a DLA or sub-DLA in each of a pair of sightlines, we construct a sample of 200 000 pairs from each of the simulated galaxies at $z = 2.3, 3.0$ and 3.6. This suite includes 100 000 sightlines from each of the face-on and edge-on renditions. In every pair, the first sightline is drawn at random from the subset known to intersect sub-DLA [log N(H I) $\geqslant$ 19.5] or DLA [log N(H I) $\geqslant$ 20.3] gas. The second sightline is drawn at random from the full simulation. In Figs 12 and 13 we show the fraction of pairs with a sub-DLA or DLA in the second line of sight,

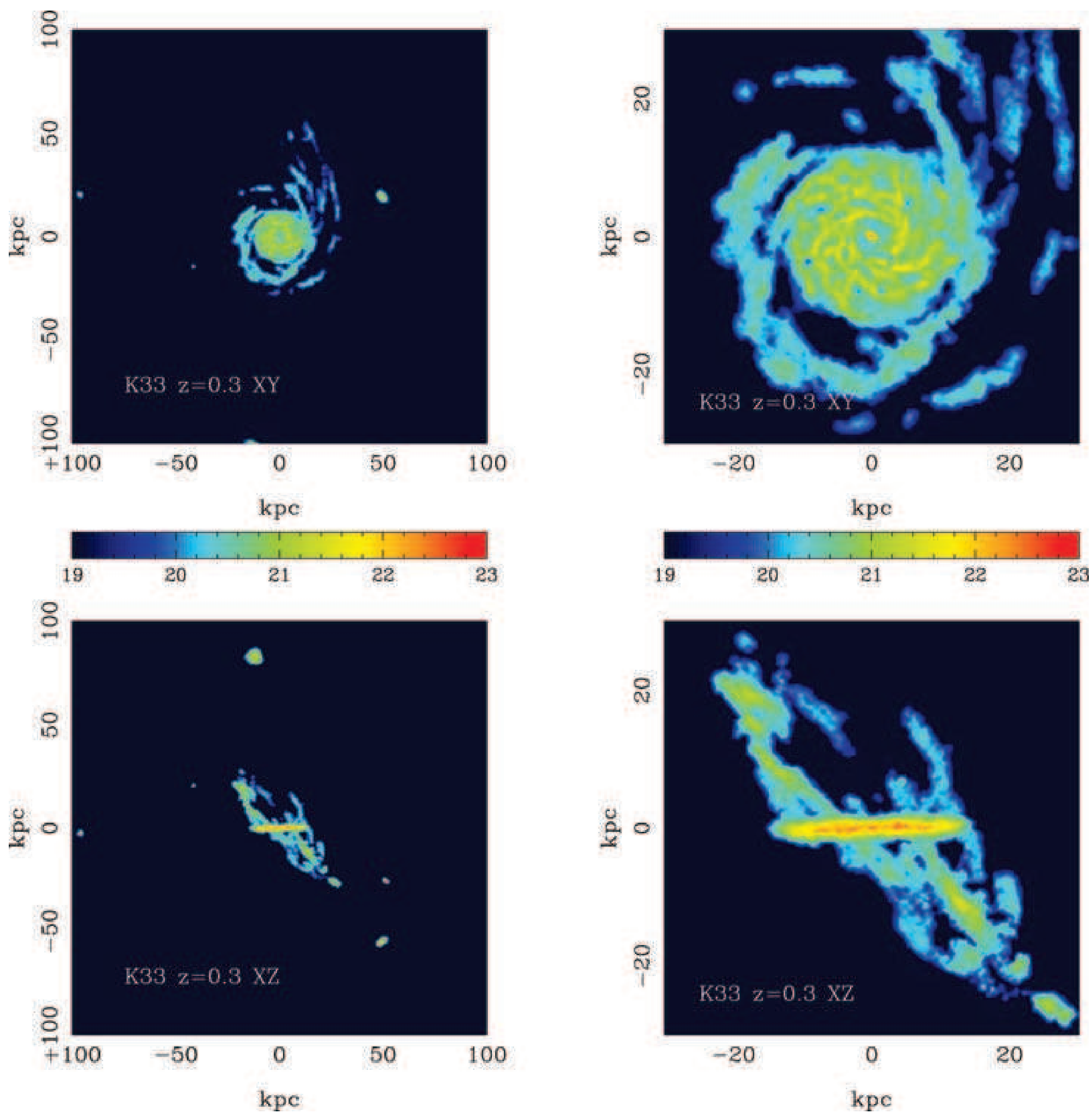

Figure 11. Projected N(H I) map for the lowest redshift slice currently simulated for galaxy K33. Two scales and two orientations are shown, as for Figs 8–10. The specific angular momentum, j, of the galaxy is 660 km s^{-1} kpc, near the median of the observed range of $j \sim$ 350–1400 kms^{-1} kpc typical for a disc galaxy of $V_c = 180$ kms^{-1} at $z \sim 0$ (e.g. Sommer-Larsen et al. 2003).

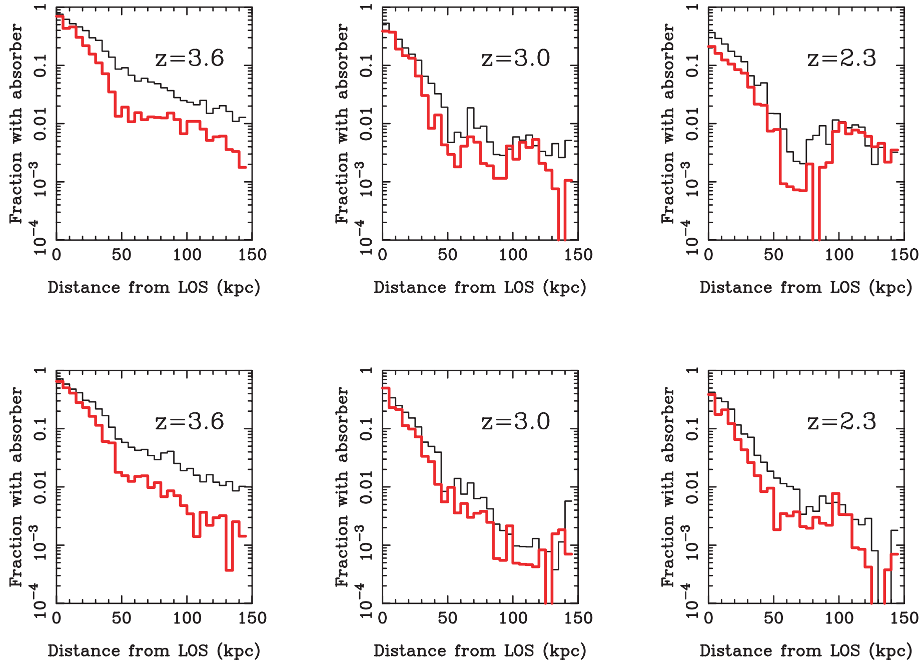

Figure 12. The fraction of second sightlines in a pair, as a function of separation, that will exhibit a DLA (red) or sub-DLA (black) given the presence of a DLA or sub-DLA in the first. This probability function for finding common absorption is calculated for three different redshifts (see panel labels) for the more massive galaxy in our simulation, K15. The top three panels are for the *XY* (face-on) orientation, and the bottom three panels are for the *XZ* (edge-on) orientation. The pair probabilities for the two orientations are very similar, as may be expected from a visual inspection of Figs 8–10.

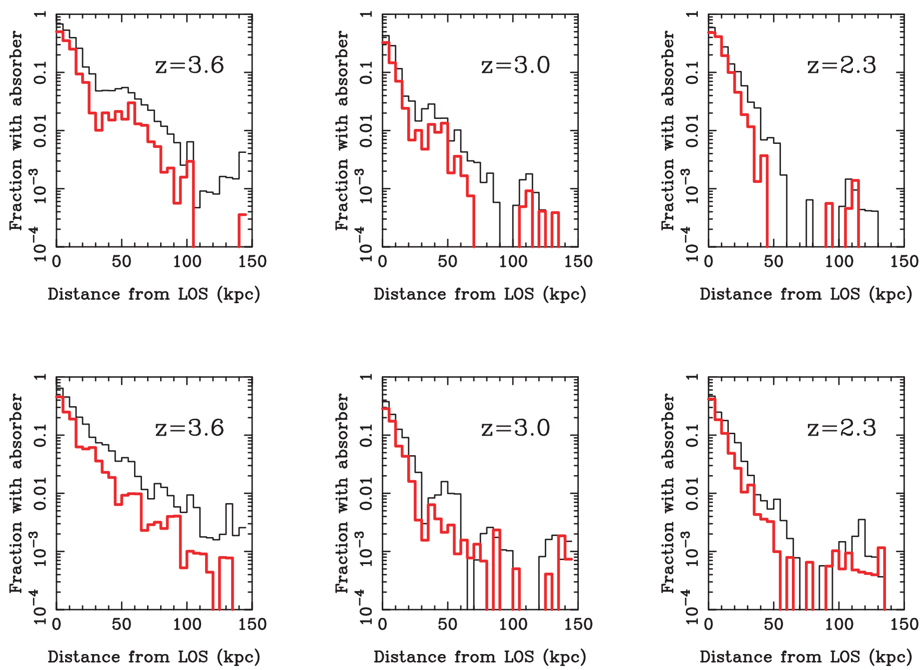

Figure 13. As for Fig. 12 but for the less massive galaxy in our simulation, K33.

given the presence of a sub-DLA or DLA in the first for galaxies K15 and K33.[4] For example, for the larger K15 galaxy at $z = 3.0$ about 6 per cent of sightlines with a DLA in the first line of sight also have a DLA in the second for separations 20–30 kpc. For sub-DLAs, this fraction increases to ~10 per cent. At separations from 40 to 150 kpc, the likelihood of finding coincident DLA absorption decreases from ~1 to 0.1 per cent in K15. In the smaller K33 galaxy, these probabilities are about a factor of 5 smaller at $z = 3.0$ and 3.6.

[4]In this simulation we classify sub-DLA as absorbers with $\log N(\mathrm{H\,I}) \geqslant 19.5$ gas, that is, grouping together classical DLAs and sub-DLAs into the same category.

In our observations of SDSS 1116+4118 AB we have one case of a sub-DLA with no counterpart in the second line of sight ($z_{\rm abs}$ = 2.47), one case of a DLA with sub-DLA counterpart ($z_{\rm abs}$ = 2.66) and one case of a pair of sub-DLAs ($z_{\rm abs}$ = 2.94) all with separations $\sim$110 h_{70}^{-1} kpc. From Figs 12 and 13 it can be seen that the probability of these two 'double hits' is $< 10^{-5}$. The present simulations still fail to reproduce the observed angular momenta of actual disc galaxies by about a factor of 1.5, and hence the real (proto)disc galaxies may be up to 50 per cent more extended than the present models. However, the probability of a double intersection is still <1 per cent at 110/1.5$\sim$75 h_{70}^{-1} kpc. Another potential uncertainty in the models is our simplified treatment of radiative transfer, which governs the transition from neutral to ionized gas and can therefore affect the effective area of projected sub-DLA absorbers. Experiments with our radiative transfer treatment indicate that this effect is likely to affect sub-DLA numbers by, at most, a factor of 2. Simulations that contain a more complete radiative transfer calculation are currently underway and will be presented in a future paper (see also Razoumov et al. 2006). Even with the uncertainties of angular momentum and the transition between neutral and ionized gas, the conclusion that a single large galaxy, such as those tested here, is unlikely to cause coincident absorption in SDSS 1116+4116 is unchanged, although tests with a larger suite of galaxies would be desirable. As the two simulation volumes also include satellites and merging components around the (proto)galaxies (e.g. bottom left-hand panel of Fig. 8), the low probability of coincident pairs found above also argues against a high covering fraction of satellite systems or an actively merging galaxy (such as that observed by Miley et al. 2006) as the explanation for the common absorption across the line of sight, at least based on these two simulated galaxies. Again, a wider suite of simulations is needed to confirm this for a more extensive parameter space.

3.2.2 *DLA clustering analysis*

Having rejected a large single system, and a galaxy plus satellite structure as the reason for coincident absorption towards SDSS 1116+4118 AB, we now consider the possibility that we are observing a structure that contains multiple galaxies. Such a possibility is perhaps not completely unexpected given that galaxy groups represent the most common environment at least at low redshift (e.g Tully 1987). Galaxy clustering at $z \sim 3$ is becoming increasingly well documented, such as the extensive literature on LBGs, for example, Giavalisco et al. (1998), Steidel et al. (1998), Porciani & Giavalisco (2002), Adelberger et al. (2005a,c), Steidel et al. (2004). Although these investigations have selected galaxies based on their emission properties, Cooke et al. (2006) have shown that DLAs have similar spatial distributions as the LBGs. DLAs may therefore also be highly clustered at $z \sim 3$. This posit is supported by recent observations of Zibetti et al. (2007) who stack images of the QSO fields of SDSS-selected Mg II absorbers. They find extended starlight out to $\sim$200 kpc, indicating that there can be galaxies at the redshift of the absorber out to these impact parameters, consistent with a group environment. Chen & Lanzetta (2003) have also found that the fields of DLAs at $z < 1$ often have multiple galaxies at the absorber redshift. We can estimate the likelihood of a multiple galaxy coincidence by considering the clustering scale of DLA galaxies and their column density distribution.

In the absence of clustering, the line density of absorption-line systems per unit redshift above the column density threshold N(H I) is given by the cosmic average $\langle \frac{{\rm d}N}{{\rm d}z} \rangle (> N({\rm H\,I}), z)$. At an average location in the universe, the probability of finding an absorber in a background quasar spectrum within the redshift interval $\Delta z = 2(1+z)\Delta v/c$, corresponding to a velocity interval $\pm\Delta v$ is simply $P = \langle {\rm d}N/{\rm d}z \rangle\ \Delta z$. For a close pair of quasar sightlines, the presence of an absorber in one of the sightlines implies an increased probability of finding an absorber at a similar redshift in the neighbouring sightline. If the quasar sightlines have a transverse separation R, and assuming that one searches a velocity interval $\pm\Delta v$ about the absorber redshift, we follow Hennawi & Prochaska (2007) and express the enhanced line density in the neighbouring sightline, $\frac{{\rm d}N}{{\rm d}z}(R, \Delta v)$, in terms of a transverse correlation function $\chi_\perp(R)$ as

$$\frac{{\rm d}N}{{\rm d}z}(R, \Delta v) = \left\langle \frac{{\rm d}N}{{\rm d}z} \right\rangle [1 + \chi_\perp(R, \Delta v)], \qquad (1)$$

where $\chi_\perp(R, \Delta v)$ is given by an average of the 3D absorber autocorrelation function, $\xi(r)$, over a cylindrical volume with cross-section A equal to the absorption cross-section, and height given by the length in the line-of-sight direction corresponding to the velocity interval $2\Delta v$. Provided that we are in the 'far-field' limit, where the transverse separation is much larger than the absorber cross-section $R \gg \sqrt{A}$, it is a very good approximation to replace the volume integral over the cylinder with a line integral over the range $L = 2\Delta v/aH(z)$, where a is the scalefactor and $H(z)$ is the Hubble constant at redshift z (see Hennawi & Prochaska 2007, for details).

Studies of the clustering of high column density absorbers, such as DLAs, are hampered by the relatively small number of absorber pairs known, which is in turn limited by the number of quasar pairs with separations smaller than the absorber autocorrelation length. These poor statistics can be circumvented if instead one cross-correlates absorbers with galaxies. Cooke et al. (2006) recently measured the clustering of LBGs around DLAs at $z \sim 3$ and measured a best-fitting cross-correlation length of $r_0 = 2.66^{+1.2}_{-1.3}\,h^{-1}$ Mpc assuming a fixed power-law slope of $\gamma = 1.6$ (see also Adelberger et al. 2003; Gawiser et al. 2001; Bouché & Lowenthal 2004). This clustering measurement is very close to the autocorrelation of LBGs, indicating that the autocorrelation of DLAs is similar in strength.

In Fig. 14 we use the Cooke et al. (2006) measurement and equation (1) to estimate the probability of detecting coincident high column density absorbers as a function of column density threshold. The lower dotted line shows the cosmic average probability $P = \langle {\rm d}N/{\rm d}z \rangle\ \Delta z$ for finding a single absorber within a $\pm$400 km s^{-1} window at redshift $z = 2.7$ in the absence of clustering. Calculating this probability requires an expression for the column density distribution $f(N)$, which we obtained by joining the $f(N)$ for DLAs log N(H I) $\geqslant$ 20.3 (Prochaska et al. 2005) with that for sub-DLAs 19 < log N(H I) < 20.3 (O'Meara et al. 2007). The solid line represents the probability for finding an absorber above a given N(H I) in a second sightline, given the presence of an absorber in the first sightline within a $\pm$400 km s^{-1} velocity window. This calculation uses the Cooke et al. (2006) best-fitting measurement for γ = 1.6 and is performed for the specific case of a 13.8 arcsec separation. The blue-shaded region represents the range permitted by the $\pm$ 1σ errors in γ quoted by Cooke et al. (2006). For this model, the probability of finding coincident sub-DLA absorption [both absorbers N(H I) > 19.5] in the SDSS 1116+4118 AB binary within a $\pm$400 km s^{-1} window is about 3 per cent. In the absence of clustering, this value is about 0.5 per cent, that is, the random probability of finding a sub-DLA in a $\pm$400 km s^{-1} velocity window based on the number density distribution alone.

The smallest separation probed by the Cooke et al. (2006) measurement is (comoving) $\sim$400 h_{70}^{-1} kpc, or about 40 per cent larger than the separation of our quasar pair sightline. The autocorrelation

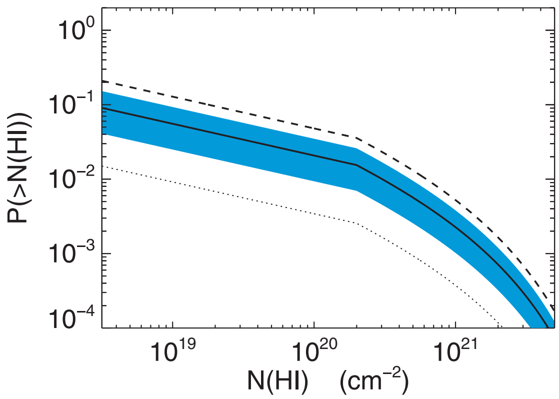

Figure 14. Probability of coincident absorption as a function of column density threshold. The lower dotted line shows the cosmic average probability for finding an absorber within a ±400 km s^{-1} window at redshift z = 2.7 in the absence of clustering. The solid line represents the probability for finding an absorber in sightline B, 13.8 arcsec away from and within ±400 km s^{-1} of an absorber detected in sightline A (or vice versa). This prediction assumes that high column density absorbers have a power-law autocorrelation function $\xi = (r/r_0)^{-\gamma}$ which is the same as the DLA–LGB correlation function measured by Cooke et al. (2006) ($\gamma = 1.6$; $r_0 = 2.66^{+1.2}_{-1.3}$), and the blue-shaded region represents their ± 1 σ errors. The dashed illustrates the effect of a steeper correlation function ($\gamma = 2.1$; $r_0 = 2.8$) which was found to be consistent with a subset of the Cooke et al. (2006) data.

functions of high-redshift galaxies tend to become progressively steeper on (comoving) scales less than about 1 h^{-1} Mpc, characteristic of the sizes of dark matter haloes (Conroy et al. 2005; Ouchi et al. 2005; Coil et al. 2006; Lee et al. 2006), and similar behaviour might be expected around the absorbers considered here. To illustrate the effect of a steeper correlation function, the dashed line in Fig. 14 shows the probability for coincident absorption for a correlation function with $\gamma = 2.11$ and $r_0 = 2.81$. This choice was motivated by the fact that Cooke et al. (2006) found that a subset of their data (11 of the 15 DLA sightlines) were best fitted with cross-correlation function parameters $\gamma = 2.11^{+1.3}_{-1.4}$ and $r_0 = 2.81^{1.4}_{2.0}$. For this model, the probability of finding coincident sub-DLA absorption [both absorbers N(H I) > 19.5] in the SDSS 1116+4118 AB binary within a 400 km s^{-1} window is about 8 per cent.

Although the probabilities that we determine from the clustering analysis are not large (<10 per cent for a single coincident pair), they are more than an order of magnitude more likely than the probability of absorption from a single large galaxy (previous subsection). Previous observations of some wide separation QSO groupings have also concluded that intervening (super)clusters may be responsible for correlated absorption (e.g. Jakobsen et al. 1986; Jakobsen, Perryman & Cristiani 1988; Francis & Hewett 1993), although the scales probed here are an order of magnitude smaller than those studies. We note that one of the coincident absorbers is separated from the systemic redshift of the QSO by ∼3000 and 4500 km s^{-1} ($z_{\rm abs}$ = 2.94 in QSO A/B, respectively). Such 'proximate' DLAs (PDLAs) have been shown to exhibit excess clustering around QSOs (Ellison et al. 2002; Russell, Ellison & Benn 2006; Prochaska, Hennawi & Herbert-Fort 2007). The probability for coincident absorption close to the QSO redshift may therefore be further enhanced beyond the calculation above.

Finally, we note that these clustering statistics are not affected by any a priori knowledge of the presence of a DLA in either sightline. The analysis *assumes* the presence of one DLA and *calculates* the probability that a matching DLA is found in the second sightline. Of course, all pairs with at least one DLA (i.e. regardless of whether there is a coincident absorber in the second sightline) should be included in order to calculate unbiased statistics. Currently, SDSS 1116+4118 AB is our only fully analysed example, although we discuss in the final section the prospects for improving these statistics.

3.3 Implications for line-of-sight observations

Regardless of the physical interpretation of the coincident absorption (single large galaxy, clustering, etc.), the correlated absorption has interesting ramifications for single line-of-sight observations. The most simplistic extrapolation of the three intervening absorbers towards this one binary system indicates that ∼2/3 of DLAs are not simple systems. From a different spatial perspective, these spatially resolved systems could be superimposed along a single sightline leading to an absorber that is a composite of two (or more) components. Whilst the consideration and treatment of complex absorption systems consisting of many superimposed 'clouds' is not new (e.g. Møller, Jakobsen & Perryman 1994; Jenkins 1986), the data presented here supply the first observational suggestion that superpositions of multiple *galaxies* may be relevant. For the velocity differences observed here (65–340 km s^{-1}) the Lyα would appear as a single trough with a column density indistinguishable from the sum of the components. Indeed, only DLAs whose relative velocities are above ∼1000 km s^{-1} would be recognized as multiple absorbers from the Lyα line alone (depending on the column densities, since higher N(H I) systems need to be separated by larger velocities for identification. Although a two-DLA blend could theoretically be identified by the asymmetry between the blue and red wings of the profile, in practice the delicate process of continuum fitting could obscure this. Difficulties include the complex underlying form of the QSO continuum (such as emission lines), flux suppression in the Lyα forest and, in the case of cross-dispersed spectra, complexity of removing the blaze, joining the orders and poor flux calibration. Indeed, when fitting the continuum around the Lyα trough of a DLA, curvature is often required to yield a normalized spectra that can be well fitted with a damped profile (e.g. Prochaska et al. 2003), which could lead to oversight of a blended absorber.

Cases of (partially) resolved multiple DLAs have previously been reported by several authors (e.g. Wolfe et al. 1986; Ellison & Lopez 2001; Lopez & Ellison 2003; Prochaska et al. 2003). Péroux et al. (2003) have also noted that 30 per cent of their sub-DLA sample is associated with another absorber. The impact of superimposed absorbers depends on a variety of factors, such as relative velocities, N(H I) and metallicities. We illustrate three possible combinations in Fig. 15. In the first scenario, a DLA is blended with a sub-DLA, both of which have the same metallicity, but due to the lower N(H I) of the sub-DLA, its metals are below the detection threshold of the spectrum, leading to an underestimate of the abundance in the blended sightline (top panel, Fig. 15). A similar underestimate would result if the velocity difference is large enough that the metal lines from the second system are not included in the fit (middle panel, Fig. 15). In practice, however, this *particular* situation is unlikely to occur since normally other, stronger, metal lines such as Fe II would signal the existence of high-velocity gas. Alternatively, if a blended sub-DLA had a higher intrinsic abundance, as has been proposed to be systematically the case (e.g. Péroux et al. 2006) we would infer an artificially high metallicity for the DLA (bottom panel, Fig. 15). Dessauges-Zavadsky et al. (2006) have noted that the abundance ratios of different velocity components in single line-of-sight DLAs are often non-uniform, which is expected if the system is a blend

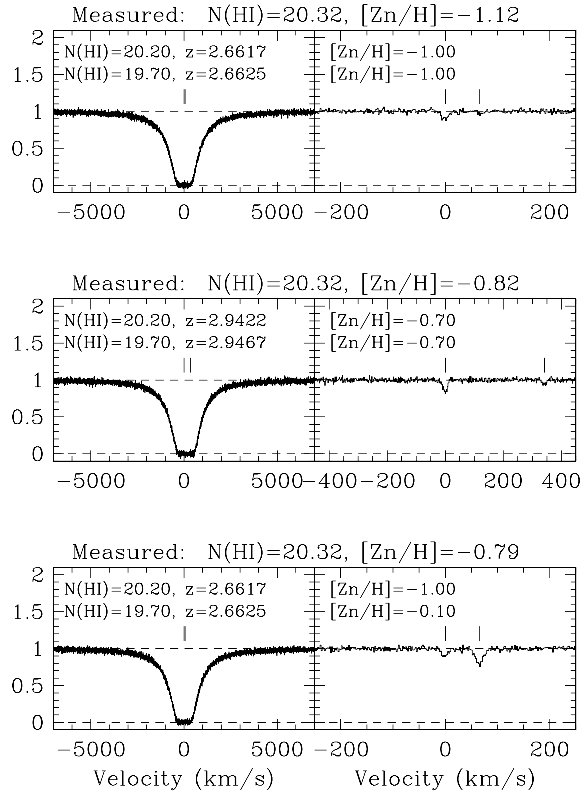

Figure 15. Illustration of the potential effect of line-of-sight blending; Lyα absorption is shown in the left-hand panels and Zn II λ 2026 is shown in the right-hand panels. In all cases, the labels within the panels show the input parameters of the two individual simulated absorbers and the labels above the panels indicates the value that would be measured for the combination of the two.

of more than one galaxy. These effects are of course most severe when the N(H I) values of the blended absorbers are close in value; a sub-DLA with log N(H I) = 19.0 will have little impact on a DLA with log N(H I) = 21.0.

The superposition of DLAs in single lines of sight may partially explain the often complex nature observed in metal line profiles and the extreme rarity of DLAs with simple velocity structures. The potential for composite absorption by multiple structures in a single line underlines the difficulty of using the kinematics of DLAs to infer their nature (Prochaska & Wolfe 1997; Haehnelt, Steinmetz & Rauch 1998).

3.4 Does a maximum likelihood estimation of absorber give an accurate DLA size?

Given the clumpy distribution of DLA column density gas in our simulated galaxies, it is interesting to ask whether statistics from pairs of QSOs can give an accurate picture of galaxy ‘size’. We therefore prepare a mock catalogue of pairs of sightlines from which we calculate a maximum likelihood estimate of absorber size based on the coincidences and anticoincidences of DLA absorption (e.g. McGill 1990; Dinshaw et al. 1997). Whilst relatively simple to implement, this technique assumes a simple geometry (usually a spherical halo or cylinder) and does not account for density fluctuations and other small-scale structure. None the less, this technique has previously been used for C IV and Mg II absorbers (Lopez et al. 2000; Ellison et al. 2004b), but the statistics are not yet available to attempt this for DLAs. For pairs of sightlines intersecting spherical clouds, the probability that a halo is intersected by the second line of sight, given that it is seen in the first, is given by

$$\phi(X) = \frac{2}{\pi}\left\{ \arccos\left[X(z)\right] - X(z)\sqrt{1 - X(z)^2}\right\} \tag{2}$$

for $0 \leqslant X(z) \leqslant 1$ and 0 otherwise. Here, $X(z) = S(z)/2R$ where $S(z)$ is the line-of-sight separation and R is the absorber radius. In order to make maximum use of the information available we actually want to calculate the probability that both lines of sight are intersected, if *either* line of sight shows absorption. This probability is given by

$$\psi = \frac{\phi}{2 - \phi}. \tag{3}$$

And the likelihood function as a function of radius is given by

$$\mathcal{L}(R) = \prod_i \psi\,[X(z_i)] \prod_j \{1 - \psi[X(z_j)]\}, \tag{4}$$

where i and j denote the number of coincidences and anticoincidences. The success of this technique relies on having a sufficient number of coincidences as well as anticoincidences to constrain the likelihood function. From a mock catalogue of 50 (half each from the XZ and XY orientations) pairs of sightlines with the impact parameter of the first DLA absorber <30 kpc from the centre of the galaxy and with all line-of-sight separations <30 kpc, we have five coincidences and 45 anticoincidences for galaxy K15 at z = 3.0 (middle left-hand panels of Figs 9 and 10). The results of the maximum likelihood analysis for this mock catalogue are shown in Fig. 16; we determine a most likely radius of $16.8^{+4.8}_{-1.4}\,h_{70}^{-1}$ kpc (95 per cent confidence limits). A smaller sample, or wider pair separations would have led to fewer coincidences and hence poorer constraints on the absorber size. A visual comparison of this most likely size with the spatial distribution of gas in Fig. 9, shows that the maximum likelihood method gives a quite reasonable estimate of the extent of DLA gas even when the distribution is clumpy; the covering fraction of gas with log N(H I) $\geqslant$ 20.3 within 16.8 kpc is ∼50 per cent. Of course, a real catalogue of pairs will likely probe galaxies of very different sizes and will therefore yield an average value. For a smoother morphology, such as the regular disc formed by the K33 galaxy at $z = 2.3$ (see bottom right-hand panel of Fig. 9) we find a most likely radius of $12.9^{+4.6}_{-2.6}$ kpc with 90 per cent of the gas within this radius above the DLA N(H I) threshold (XY plane).

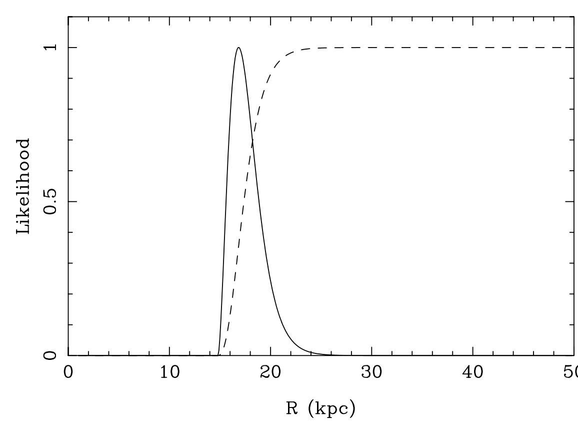

Figure 16. Maximum likelihood distribution (solid line) and cumulative distribution (dashed line) of the size of DLA absorbing gas from a mock catalogue of 50 pairs of sightlines for galaxy K15 at z = 3.0. The most likely radius from this simulated catalogue is found to be 16.8 h_{70}^{-1} kpc with 95 per cent confidence limits of 15.4 and 21.6 h_{70}^{-1} kpc.

The compilation of a sample of 50 pairs with separations <30 kpc (∼4 arcsec) in which at least one DLA is detected is a considerable challenge. However, the required number of pairs is fewer if the separations are also smaller, because coincidences will be detected at a higher rate and therefore constrain the absorber size better for a smaller sample. For example, if we repeat the maximum likelihood analysis described above for the K15 galaxy at $z = 3.0$, but with a maximum pair separation of 20 kpc, from four coincidences and 16 anticoincidences we deduce a most likely radius of $13.2^{+10.5}_{-2.5}$ kpc. This means that if the simulations we have used in this work are a reasonably accurate representation of the size of the DLA cross-section in high-redshift galaxies, close pairs with separations <3 arcsec or wide separation lenses will be best able to observationally constrain DLA size.

4 CONCLUSIONS

We have presented moderate resolution spectra of a pair of QSOs at $z \sim 3$ separated by 13.8 arcsec on the sky. DLA or sub-DLA absorption is identified at three intervening redshifts: $z_{\rm abs} = 2.47, 2.66$ and 2.94. For the two higher redshift systems, absorption is seen in both lines of sight which have proper transverse separations of $\sim 110\ h_{70}^{-1}$ kpc. We measure chemical abundances for three of the five absorbers detected in our ESI spectra and determine high metallicities for two of them: 1/5 and 1/3 $Z_{\odot}$. Both absorbers also have quite high dust depletions and for the $z_{\rm abs} = 2.94$ DLA we also find that there is no α element enhancement, [S/Zn] = +0.05, and measure a low fraction of molecular gas, $\log f({\rm H}_2) < -5.5$ in this particular line of sight.

Although this is the first time that transverse DLA absorption on this scale has been studied, if line-of-sight blending occurs as often as the coincidences observed in SDSS 1116+4118 AB, we demonstrate that this could have important ramifications. For example, the determination of chemical abundances can be affected by several tenths of a dex and kinematics become challenging to interpret. Although more QSO pairs with separations of a few tens to a few hundreds of kpc are clearly required to confirm whether blending may really occur frequently in single line-of-sight DLAs, our work identifies a potential complication in the interpretation of DLA properties.

This is the first time that DLAs have been studied on a transverse scale $>10\ h_{70}^{-1}$ kpc and offers an opportunity to study their size and environment. By producing artificial pairs of sightlines through high-resolution galaxy simulations, we conclude that the coincident absorption is unlikely to be associated with a single large galaxy, or a galaxy plus satellite system. Instead, from a clustering analysis, we find that the statistically more likely scenario is one in which the binary sightlines intersect multiple galaxies. However, the probability for coincident sub-DLA absorption is still <10 per cent, so more observations of QSO pairs are required to more robustly interpret our data.

The prospects for extending the analysis of absorption in QSO pairs are promising, thanks to the large sky coverage of the SDSS. Hennawi et al. (2006b) estimate that the current 8000 deg^2 of SDSS imaging contains ∼140 pairs with $\Delta\theta < 25$ arcsec and $z > 1.8$. Many of these will require follow-up spectroscopy since the blue coverage of the SDSS spectra only reaches down to $z_{\rm abs} \sim 2.2$. However, based on absorber number densities, Hennawi et al. (2006b) estimate that the SDSS sample of pairs would contain ∼70 sub-DLAs or DLAs. Measuring the rate of coincident absorption in a sample of this size may, at last, place the scale of DLA absorption and the structure of its environment on solid ground.

ACKNOWLEDGMENTS

The ESI spectra were reduced using software written by Jason X. Prochaska, who was generous with his time and advice during the data reduction process. SLE acknowledges the hospitality of the Dark Cosmology Centre in Copenhagen where some of this work was done. JFH is supported by NASA through Hubble Fellowship grant # 01172.01-A awarded by the Space Telescope Science Institute, which is operated by the Association of Universities for Research in Astronomy, Inc., for NASA, under contract NAS 5-26555. CLM is supported by the David and Lucile Packard Foundation. We acknowledge useful discussions with Alexei Razoumov and John O'Meara. The TreeSPH simulations were performed on the SGI Itanium II facility provided by DCSC. The Dark Cosmology Centre is funded by the DNRF. The data presented herein were obtained at the W. M. Keck Observatory, which is operated as a scientific partnership among the California Institute of Technology, the University of California and the National Aeronautics and Space Administration. The Observatory was made possible by the generous financial support of the W. M. Keck Foundation. The authors wish to recognize and acknowledge the very significant cultural role and reverence that the summit of Mauna Kea has always had within the indigenous Hawaiian community. We are most fortunate to have the opportunity to conduct observations from this mountain.

REFERENCES

Adelberger K., Steidel C. C., Shapley A. E., Pettini M., 2003, ApJ, 584, 45

Adelberger K., Erb D. K., Steidel C. C., Reddy N. A., Pettini M., Shapley A. E., 2005a, ApJ, 620, L75

Adelberger K., Shapley A. E., Steidel C. C., Pettini M., Erb D., Reddy N. A., 2005b, ApJ, 629, 636

Adelberger K., Steidel C. C., Pettini M., Shapley A. E., Reddy N. A., Erb D. K., 2005c, ApJ, 619, 697

Adelberger K., Steidel C. C., Kollmeier J. A., Reddy N. A., 2006, ApJ, 637, 74

Akerman C. J., Ellison S. L., Pettini M., Steidel C. C., 2005, A&A, 440, 499

Bonifacio P., Sbordone L., Marconi G., Pasquini L., Hill V., 2004, A&A, 414, 503

Bouché N., Lowenthal J. D., 2004, ApJ, 609, 513

Bowen D. V., Pettini M., Blades J. C., 2002, ApJ, 580, 169

Briggs F. H., Wolfe A. M., Liszt H. S., Davis M. M., Turner K. L., 1989, ApJ, 341, 650

Chen H.-W., Lanzetta K., 2003, ApJ, 597, 706

Chen H.-W., Kennicutt R., Rauch M., 2005, ApJ, 620, 703

Churchill C. W., Mellon R. R., Charlton J. C., Vogt S., 2003, ApJ, 593, 203

Churchill W. C., Kacprzak G., Steidel C. C., 2005, in Williams P. R., Shu C., Ménard B., eds, Proc. IAU 199, Probing Galaxies through Quasar Absorption Lines. Cambridge Univ. Press, Cambridge, p. 24

Coil A. L., Newman J. A., Cooper M. C., Davis M., Faber S. M., Koo D. C., Willmer C. N. A., 2006, ApJ, 644, 671

Conroy C. et al., 2005, ApJ, 635, 982

Cooke J., Wolfe A. M., Gawiser E., Prochaska J. X., 2006, ApJ, 636, L9

Dessauges-Zavadsky M., Calura F., Prochaska J. X., D'Odorico S., Matteucci F., 2004, A&A, 416, 79

Dessauges-Zavadsky M., Prochaska J. X., D'Odorico S., Calura F., Matteucci F., 2006, A&A, 445, 93

Dinshaw N., Weymann R., Impey C., Foltz C. B., Morris S. L., Ake T., 1997, ApJ, 491, 45

Ellison S. L., Lopez S., 2001, A&A, 380, 117

Ellison S. L., Yan L., Hook I., Pettini M., Wall J., Shaver P., 2001, A&A, 379, 393

Ellison S. L., Yan L., Hook I., Pettini M., Wall J., Shaver P., 2002, A&A, 383, 91
Ellison S. L., Churchill C. W., Rix S. A., Pettini M., 2004a, ApJ, 615, 118
Ellison S. L., Ibata R., Pettini M., Lewis G. F., Aracil B., Petitjean P., Srianand R., 2004b, A&A, 414, 79
Ellison S. L., Hall P. B., Lira P., 2005a, AJ, 130, 1345
Ellison S. L., Kewley L. J., Mallén-Ornelas G., 2005b, MNRAS, 357, 354
Erb D. K., Shapley A. E., Steidel C. C., Pettini M., Adelberger K. L., Hunt M. P., Moorwood A. F. M., Cuby J.-G., 2003, ApJ, 591, 101
Erb D. K., Steidel C. C., Shapley A. E., Pettini M., Adelberger K. L., 2004, ApJ, 612, 122
Erb D. K., Shapley A. E., Pettini M., Steidel C. C., Reddy N. A., Adelberger K. L., 2006, ApJ, 644, 813
Foltz C. B., Chaffee F. H., Wolfe A. M., 1988, ApJ, 335, 35
Francis P., Hewett P., 1993, AJ, 105, 1633
Fynbo J. U., Møller P., Warren S. J., 1999, MNRAS, 305, 849
Gawiser E., Wolfe A., Prochaska J., Lanzetta, Yahata N., Quirrenbach A., 2001, ApJ, 562, 628
Giavalisco M., Steidel C. C., Adelberger K. L., Dickinson M. E., Pettini M., Kellogg M., 1998, ApJ, 503, 543
Gratton R., Carretta E., Claudi R., Lucatello S., Barbieri M., 2003, A&A, 404, 187
Haardt F., Madau P., 1996, ApJ, 461, 20
Haehnelt M. G., Steinmetz M., Rauch M., 1998, ApJ, 495, 647
Hennawi J. F., Prochaska J. X., 2007, ApJ, 655, 735
Hennawi J. F. et al., 2006a, AJ, 131, 1
Hennawi J. F. et al., 2006b, ApJ, 651, 61
Herbert-Fort S., Prochaska J. X., Dessauges-Zavadsky M., Ellison S. L., Howk J. C., Wolfe A. M., Prochter G. E., 2006, PASP, 118, 1077
Inada N. et al., 2003, Nat, 426, 810
Jakobsen P., Perryman M. A. C., di Serego Alighieri S., Ulrich M. H., Macchetto F., 1986, ApJ, 303, L27
Jakobsen P., Perryman M. A. C., Cristiani S., 1988, ApJ, 326, 710
Jenkins E. B., 1986, ApJ, 304, 739
Jorgenson R., Wolfe A. M., Prochaska J. X., Lu L., Howk J. C., Cooke J., Gawiser E., Gelino D., 2006, ApJ, 646, 730
Kobayashi N., Terada H., Goto M., Tokunaga A., 2002, ApJ, 569, 676
Kroupa P., 1998, MNRAS, 298, 231
Labbé I. et al., 2003, ApJ, 591, L95
Lanzetta K., 1993, in Shull J. M., Thronson H. A., eds, The Environment and Evolution of Galaxies. Kluwer, Dordrecht, p. 237
Ledoux C., Petitjean P., Srianand R., 2003, MNRAS, 346, 209
Lee K.-S., Giavalisco M., Gnedin O. Y., Somerville R. S., Ferguson H. C., Dickinson M., Ouchi M., 2006, ApJ, 642, 63
Lia C., Portinari L., Carraro G., 2002a, MNRAS, 330, 821
Lia C., Portinari L., Carraro G., 2002b, MNRAS, 335, 864
Lodders K., 2003, ApJ, 591, 1220
Lopez S., Ellison S. L., 2003, A&A, 403, 573
Lopez S., Hagen H.-J., Reimers D., 2000, A&A, 357, 37
Lopez S., Reimers D., Gregg M. D., Wisotzki L., Wucknitz O., Guzman A., 2005, ApJ, 626, 767
McGill C., 1990, MNRAS, 242, 544
Meiring J., Kulkarni V. P., Khare P., Bechtold J., York D. G., Cui J., Lauroesch J. T., Crotts A. P. S., Nakamura O., 2006, MNRAS, 370, 43
Miley G. K. et al., 2006, ApJ, 650, L29
Møller P., Jakobsen P., Perryman M. A. C., 1994, A&A, 287, 719
Møller P., Fynbo J. P. U., Fall S. M., 2004, A&A, 422, L33
Monaghan J. J., Lattanzio J. C., 1985, A&A, 149, 135
Nissen P. E., Chen Y. Q., Asplund M., Pettini M., 2004, A&A, 415, 993
Oguri M. et al., 2004, ApJ, 605, 78
O'Meara J. M., Prochaska J. X., Burles S., Prochter G., Bernstein R. A., Burgess K. M., 2007, ApJ, 656, 666
Ouchi M. et al., 2005, ApJ, 635 L117
Péroux C., Dessauges-Zavadsky M., D'Odorico S., Kim T.-S., McMahon R., 2003, MNRAS, 345, 480
Péroux C., Meiring J. D., Kulkarni V. P., Ferlet R., Khare P., Lauroesch J. T., Vladilo G., York D. G., 2006, MNRAS, 372, 369
Petitjean P., Ledoux C., Noterdaeme P., Srianand R., 2006, A&A, 456, L9
Pettini M., Smith L. J., King D. L., Hunstead R. W., 1997, ApJ, 486, 665
Pettini M., Ellison S. L., Steidel C. C., Bowen D. V., 1999, ApJ, 510, 576
Pettini M., Rix S., Steidel C., Adelberger K., Hunt M., Shapley A., 2002, ApJ, 569, 742
Pieri M. M., Schaye J., Aguirre A., 2006, ApJ, 638, 45
Pompéia L., Hill V., Spite M., 2005, Nucl. Phys. A, 758, 242
Porciani C., Giavalisco M., 2002, ApJ, 565, 24
Prochaska J. X., Wolfe A. M., 1997, ApJ, 487, 73
Prochaska J. X., Gawiser E., Wolfe A. M., Cooke J., Gelino D., 2003, ApJS, 147, 227
Prochaska J. X., Herbert-Fort S., Wolfe A. M., 2005, ApJ, 635, 123
Prochaska J. X., Hennawi J. F., Herbert-Fort S., 2007, ApJ, submitted (astro-ph/0703594)
Rauch M., Sargent W. L. W., Barlow T. A., 2001a, ApJ, 554, 823
Rauch M., Sargent W. L. W., Barlow T., Carswell R. F., 2001b, ApJ, 562, 76
Razoumov A. O., Sommer-Larsen J., 2006, ApJ, 651, L89
Razoumov A. O., Norman M. L., Prochaska J. X., Wolfe A. M., 2006, ApJ, 645, 55
Robertson B., Yoshida N., Springel V., Hernquist L., 2004, ApJ, 606, 32
Roth K. C., Blades J. C., 1997, ApJ, 474, L95
Russell D., Ellison S. L., Benn C. R., 2006, MNRAS, 367, 412
Sanchez-Alvaro E., Rodriguez-Calonge F. J., 2007, preprint (astro-ph/0701537)
Savage B. D., Sembach K. R., 1991, ApJ, 379, 245
Savage B. D., Sembach K. R., 1996, ARA&A, 34, 279
Savaglio S. et al., 2005, ApJ, 635, 260
Shapley A. E., Erb D. K., Pettini M., Steidel C., Adelberger K., ApJ, 2004, 612, 108
Sheinis A. I., Bolte M., Epps H. W., Kibrick R. I., Miller J. S., Radovan M. V., Bigelow B. C., Sutin B. M., 2002, PASP, 114, 851
Shetrone M., Venn K. A., Tolstoy E., Primas F., Hill V., Kaufer A., 2003, AJ, 125, 684
Smette A., Robertson J. G., Shaver P., Reimers D., Wisotzki L., Kohler Th., 1995, A&AS, 113, 199
Sommer-Larsen J., 2006, ApJ, 644, L1
Sommer-Larsen J., Götz M., Portinari L., 2003, ApJ, 596, 46
Springel V., Hernquist L., 2002, MNRAS, 333, 649
Steidel C. C., 1993, in Shull J. M., Thronson H. A., eds, Astrophys. Space Sci. Library Vol. 188, The Environment and Evolution of Galaxies. Springer, New York, p. 263
Steidel C. C., 1995, in Meylan ed., ESO Workshop, QSO Absorption Lines. p. 139
Steidel C. C., Adelberger K. L., Dickinson M., Giavalisco M., Pettini M., Kellogg M., 1998, ApJ, 492, 428
Steidel C. C., Shapley A., Pettini M., Adelberger K., Erb D., Reddy N., Hunt M., 2004, ApJ, 604, 534
Teplitz H. et al., 2000, ApJ, 542, 18
Tremonti C. et al., 2004, ApJ, 693, 898
Tully R. B., 1987, ApJ, 321, 280
Tumlinson J. et al., 2002, ApJ, 566, 857
Weatherley S. J., Warren S. J., Møller P., Fall S. M., Fynbo J. U., Croom S. M., 2005, MNRAS, 358, 985
Wolfe A. M., Chen H.-W., 2006, ApJ, 652, 981
Wolfe A. M., Turnshek D. A., Smith H. E., Cohen R. D., 1986, ApJS, 61, 249
York D. G. et al., 2006, MNRAS, 367, 945
Zibetti S., Menard B., Nestor D. B., Quider A. M., Rao S. M., Turnshek D. A., 2007, ApJ, 658, 161
Zwaan M. A., Meyer M. J., Staveley-Smith L., Webster R. L., 2005, MNRAS, 359, 30

This paper has been typeset from a TEX/LATEX file prepared by the author.